Author Query

Methods in Cell Biology, 88
Article No.: Chapter 12

Dear Author,

During the preparation of your manuscript for typesetting some questions have arisen. These are listed below. Please check your typeset proof carefully and mark any corrections in the margin of the proof or compile them as a separate list. This form should then be returned with your marked proof/list of corrections to Elsevier Science.

Disk use

In some instances we may be unable to process the electronic file of your article and/or artwork. In that case we have, for efficiency reasons, proceeded by using the hard copy of your manuscript. If this is the case the reasons are indicated below:

☐ Disk damaged ☐ Incompatible file format ☐ LaTeX file for non-LaTeX journal

☐ Virus infected ☐ Discrepancies between electronic file and (peer-reviewed, therefore definitive) hard copy.

☐ Other: .....

We have proceeded as follows:

☐ Manuscript scanned ☐ Manuscript keyed in ☐ Artwork scanned

☐ Files only partly used (parts processed differently:.....)

Bibliography

If discrepancies were noted between the literature list and the text references, the following may apply:

☐ The references listed below were noted in the text but appear to be missing from your literature list. Please complete the list or remove the references from the text.

☐ Uncited references: This section comprises references which occur in the reference list but not in the body of the text. Please position each reference in the text or, alternatively, delete it. Any reference not dealt with will be retained in this section.

Query Refs.	Details Required	Author's response
AU1	Please provide the volume number and page range for the reference "Uribe and Jay, 2007" in the list.	
AU2	Heuser and Salpeter, 1979 is not provided in the reference list. Please supply.	
AU3	Suzuki *et al.*, 2005 is not provided in the reference list. Please supply.	
AU4	Please check the chapter title.	

Molecular and Cellular Neuroscience 39 (2008) 465–477

Contents lists available at ScienceDirect

Molecular and Cellular Neuroscience

journal homepage: www.elsevier.com/locate/ymcne

Balanced expression of various TrkB receptor isoforms from the *Ntrk2* gene locus in the mouse nervous system

Haruko Kumanogoh *, Junko Asami, Shun Nakamura, Takayoshi Inoue

Department of Biochemistry and Cellular Biology, National Institute of Neuroscience, National Center of Neurology and Psychiatry, 4-1-1 Ogawahigashi, Kodaira, Tokyo 187-8502, Japan

ARTICLE INFO

Article history:
Received 21 March 2008
Revised 23 July 2008
Accepted 30 July 2008
Available online 9 August 2008

Keywords:
TrkB
BDNF
Alternative splicing
Antisense transcript
Mouse nervous system

ABSTRACT

A brain-derived neurotrophic factor (BDNF) receptor TrkB involves three spliced variants, namely the tyrosine kinase domain (TK) intact (+) and two TK(−) isoforms T1 and T2, yet their precise roles are largely unknown. Here we extensively map the mRNA expression patterns of BDNF and TrkB variants, further to gain insights in TK(−) specific functions during mouse development. Consequently, we found that TK(+), T1 and T2 were expressed in distinct regions of the mouse nervous system at the embryonic and postnatal stages, implicating separable functions of TK(−) forms. Additionally we uncovered five expressed segments in the intron between T2 and T1 specific exons, and one of these segments was revealed to code novel TK(−) receptors with unique responsiveness *in vitro*. These results suggest dynamic modes of expression from the *Ntrk2* gene locus and multiple roles of TK(−) forms in the developing mouse nervous system.

Introduction

Brain-derived neurotrophic factor (BDNF) is a member of nerve growth factor (NGF) family that supports survival and differentiation of selected neuronal populations both in the central and peripheral nervous systems during development. BDNF is also known to play multiple roles in axonal pathfindings, dendritic growth and/or synaptic plasticity at the perinatal to adult stages (Bibel and Barde, 2000; Blum and Konnerth, 2005; Poo, 2001). In mice, for instance, three groups have independently generated *BDNF* gene knockout mice to reveal *in vivo* roles of BDNF (Conover et al., 1995; Ernfors et al., 1995; Jones et al., 1994; Liu et al., 1995) and found that *Bdnf*(−/−) mice are born alive but mostly died within 20 days after birth. They also realized abnormal behaviors of *Bdnf*(−/−) mice including difficulty in righting and spinning (Conover et al., 1995; Ernfors et al., 1995; Jones et al., 1994). At the tissue and cellular level, *Bdnf*(−/−) mice had massive cell loss in the peripheral sensory ganglia such as the dorsal root ganglia and trigeminal ganglia, while no significant cell loss was evident in the facial or spinal motor neurons. In contrast to the defects observed in the peripheral structures, no significant cytoarchitectural abnormalities were recognizable in the brain of knockout mice, although the mutant brain was smaller than control one (Conover et al., 1995). It was further found out that certain subpopulations of neurons were affected fully in differentiation (Itami et al., 2007; Jones et al., 1994), which suggests that BDNF is important in regulating differentiation of these neurons rather than cell survival. In human, accumulated evidence has indicated that *BDNF* mutations could be a causative factor of neurodegenerative disorders such as Alzheimer's, Huntington's and Parkinson diseases (Conover et al., 1995; Murer et al., 2001; Siegel and Chauhan, 2000; Zuccato and Cattaneo, 2007). Most recently, roles of alternative promoters in regulated expression BDNF have been elucidated, implicating context dependent activation of BDNF signaling machineries with multiple receptor components (Chiaruttini et al., 2008).

Tropo-myosine-related kinase (Trk) B is one of well characterized membrane components for BDNF receptors that are highly expressed in the nervous system (Klein et al., 1989). Its extracellular region consists of a signal peptide, two cysteine-rich domains, a cluster of three leucine-rich motifs, and two immunoglobulin-like domains, while its intracellular domain contains the tyrosine kinase domain (as illustrated in Fig. 5B). Thus far, three TrkB splicing variants have been identified in rat (Middlemas et al., 1991); a tyrosine kinase intact form (TK(+)) and two kinase truncated forms (TK(−): T1 and T2). T1 and T2 have unique short C-terminal amino acid sequences (T1, 11 residues; T2, 9 residues) instead of the tyrosine kinase domain of TK(+). TK(+) was identified in various species including mammals, chick, frog and zebrafish, and many studies have revealed the signal transduction pathways (Reichardt, 2006), expression profiles and functions. In mice, two kinds of TrkB gene knockout organisms have been generated (Klein et al., 1993; Luikart et al., 2003). One is *TrkB*^{k}(−/−), the TK(+) isoform-specific knockout mice, and the other is *TrkB*(−/−) to delete all TrkB isoforms in mice. Both mice were born alive but mostly died within 4 days because they were unable to take nourishment. *TrkB*^{k}(−/−) mice had cell loss in both the sensory and motor neurons and these phenotypes were severer than those in *Bdnf* gene knockout mice in which only the sensory neurons were affected. This indicated that TrkB uses other neurotrophins as its ligand in *in vivo* situations. In *TrkB*(−/−) mice, the cell loss phenotype of sensory

* Corresponding author. Fax: +81 42 346 1752.
E-mail address: kumanogo@ncnp.go.jp (H. Kumanogoh).

1044-7431/$ – see front matter © 2008 Elsevier Inc. All rights reserved.
doi:10.1016/j.mcn.2008.07.024

neurons was severer than that in *TrkB*^{k}(−/−) mice, particularly in those regions where survival of neurons is totally dependent on BDNF and neurotrophin-3, implicating functional relevance of multiple kinds of TrkB receptor isoforms other than the TK(+) isoform.

TK(−) variants had been assumed to simply play a dominant negative role on TK(+) (Eide et al., 1996; Haapasalo et al., 2001; Li et al., 1998). However, one of TK(−) isoform, TrkB-T1 receptor was identified in mouse, monkey, human and chick, and recently, others and we have shown that T1 isoform alone could activate a discrete signaling cascade in rat astrocytes; T1 has a direct signaling role in mediating inositol-1,4,5-triphosphate-dependent calcium release (Rose et al., 2003), and T1 isoform alone could activate a discrete signaling cascade by a cytoplasimic binding partner RhoGDI1 to reorganize cytoskeletons (Ohira et al., 2005). On the other hand, T2 isoform has been deposited to the public database only in rat. Two groups have reported T2 transcript and protein expressions: Armanini et al. reported that mRNAs encoding two truncated isoforms, TrkB-T1 and -T2, are differently distributed in the rodent nervous system, and each of these transcripts is co-expressed with TK(+) (Armanini et al., 1995). Silhol et al. demonstrated that T2 mRNA and its protein product gradually decreased from the postnatal day-7 becoming undetectable by 22-month-old in the rat hippocampi by the RNA protection assay and western blot analysis using specific antisera for rat T2 isoform, while physiological properties of T2 are still largely unknown. In any cases, *in vivo* roles of TK(−) remain uncertain (Silhol et al., 2005).

To further understand *in vivo* functions of TK(−) during mouse development, it would be important to identify those cell populations that express each TrkB isoform. In the present study, we extensively map mRNA expression patterns of BDNF and TrkB variants by a sensitive *in situ* hybridization (ISH) method. As the results, we found that TK(−) mRNA expression did occur in TK(+) negative cell populations both at the embryonic and postnatal stages. In addition, we realized differential expression profiles of T1 and T2 transcripts along the ventricular zone of the embryonic and postnatal brains. These results implicate novel and separable roles of TK(−) forms in regulating cell division and/or differentiation of the ventricular/ependymal cells. Furthermore, we found some bidirectionally transcribed regions located within an *Ntrk2* gene intron and identified novel TrkB splicing variants from one of the transcribed regions of *Ntrk2* by means of RT-PCR. Importantly, each expressed TrkB isoform in Neuro-2a cells appeared to be delivered to distinct subcellular domains and more or less affect cell shapes. These results highlight intricate modes of *Ntrk2* gene expression and multiple roles of TK(−) variants in neural development.

Results

Confirmation of mouse Ntrk2 gene structure to design specific ISH probes for TrkB isoforms

To investigate *in vivo* roles of TK(−), we first tried to precisely map the expression patterns of TrkB isoforms and their ligand, BDNF by means of a sensitive *in situ* hybridization (ISH) in the mouse nervous system. To obtain specific ISH probes for each TrkB receptor isoform, we referred to the UCSC genome browser (http://genome.ucsc.edu) and confirmed the structure of mouse *Ntrk2* gene locus that generates TrkB receptor isoforms. As was summarized in Fig. 1A, nine exons from the second to tenth only encode the extracellular (EC) region, the eleventh exon encodes both the EC and transmenbrane (TM) region (colored in red), the twelfth exon encodes the TM and a part of juxtamembrane region (JM) (colored in gray) and the last six exons (colored in pink) encode the tyrosine kinase (TK) domain containing cytoplasmic region of mouse TrkB-TK(+) isoform in the gene locus.

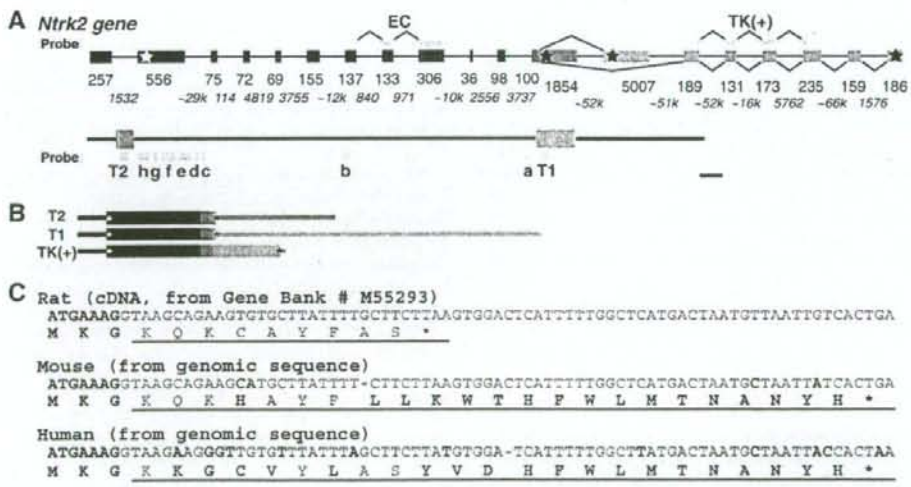

Fig. 1. Genomic organization of the *Ntrk2* (TrkB) locus and its alternative transcripts. (A) The upper illustration shows structure of the *Ntrk2* gene locus. Exons and introns are depicted as boxes and horizontal lines respectively. The alternative splicing patterns are represented by solid v-shapes connecting the exons. The numbers indicate their sizes by base pairs (those numbers in italics are for introns). Constitutive exons are specified as black, red and gray boxes, while alternative exons are shown as colored boxes: TK(+); pink, T1; green, T2; blue. The red and gray boxes show transmembrane and juxtamembrane region-coding domains, respectively. White and black stars show positions of the initiation and stop codons respectively. The lower drawing is a higher magnification between T2 and T1 exons. Bar represents 2 kb. *In situ* hybridization (ISH) probes in this study are indicated by orange boxes. Probes for the extracellular domain (EC) and TK domain (TK) cover coding regions straddling more than two exons. Probes a, b, c, d, e, f, g and h are positioned in the intron between the last constitutive exon and T1 exon. BDNF probe is against the part of the coding region (not shown). (B) Mature transcripts from the *Ntrk2* gene locus generated by alternative splicing. Translated regions are shown by colored boxes and untranslated segments are shown by colored lines. White and black stars show positions of the initiation and stop codons respectively. (C) Comparison of T2 amino acid sequences among species. Those amino acid (a.a.) sequences based on rat cDNA and mouse or human genomic DNA sequences are aligned. The constitutive exon and continuous T2 specific regions are shown in black and blue, respectively. Letters written in red indicate deletion or substitution nucleotides and distinct a.a. sequences compared with rat ones. T2 specific a.a. sequences are underlined. Note that putative T2 a.a. sequences are not well conserved among mammals.

Between the TM–JM specific exon and the first cytoplasmic specific exon of TrkB-TK(+), one alternative exon is annotated. This exon is shown by a green box in Fig. 1A, standing as a totally isolated alternative exon encoding T1 specific cytoplasmic tail. Based on the information, we selected those exonic regions encoding a part of TrkB extracellular immunoglobulin-like domains as the EC probe to detect all TrkB isoforms as was previously reported (Klein et al., 1989). T1 isoform-specific probe was prepared from its specific exon and TK probe was employed to avoid cross-react with other Trk family members as previously described (Armanini et al., 1995; McMahon et al., 1994).

In designing T2 isoform-specific probe, we initially referred to the cDNA sequence that was only reported in rat (Middlemas et al., 1991): we found that the rat T2 specific exon is located at the 3′-flanking region of the last TrkB constitutive exon (=TM–JM specific exon) without any intronic gaps. Synthesis of mature mRNAs for rat TrkB splicing variants has therefore been assumed as follows; immature RNAs are first transcribed from the rat *Ntrk2* gene locus, then constitutive exons (as shown with black boxes in Fig. 1A) and alternative exons, namely T2 (a blue box in Fig. 1A), T1 (a green box in Fig. 1A), or TK (pink boxes in Fig. 1A), are selected by splicing, and mature T2, T1 or TK(+) mRNAs are finally synthesized, respectively (the schematic drawings of spliced mature mRNAs were shown in Fig. 1B). We next predicted mouse and human putative T2 amino acid sequences from their genomic sequences based on the rat T2 exonic position, and these deduced amino acid sequences were compared with the rat T2 protein tail structure. Unexpectedly, these isoform-specific amino acid sequences and lengths were totally different as shown in Fig. 1C; rat; 9 amino acids, mouse and human; 23 amino acids, while T1 tail structure was well conserved among mouse, rat, human, monkey and chick (data not shown). This indicates a possibility that T2 transcript is merely a part of premature mRNAs for other TrkB isoforms and is not to be translated to the protein at all. ISH probe for mouse T2 segment was hence prepared from the mouse genomic sequence corresponding to rat T2 genomic position. We additionally developed two intronic probes a and b to compare the expression profiles with those obtained by T2 probe. One of intronic probes, probe a, covers the 5′-flanking region of T1 exon and the other, probe b, is situated in the middle of two exons (Fig. 1A). To gain identical level of signals in case these intronic regions and T2 segment have equal level of expressions, we conferred same length and UTP ratio to these probe sequences. By using these probe sets, we could determine if T2 is a part of immature mRNA for other TrkB isoforms or not, as the T2 specific region is considered to be a portion of the intron between the last 3′-constitutive exon and T1 exon. For instance, T2 segment is considered as a part of the intron when these two intronic probes yield the same signal levels as T2 probe. T2 segment is regarded as an exon for a TrkB isoform when T2 expression profile is totally different from expression signals detected with these two intronic probes.

Distinct expression profiles of TrkB isoforms and BDNF during mouse development

We compared the expression patterns of BDNF, TrkB isoforms; TK(+), T1, T2, two intronic regions (a and b) and all TrkB isoforms detected by the EC probe at the three mouse developmental stages, embryonic 12.5-day (E12.5), postnatal day-7 (P7) and 8-week-old (8W) by means of ISH on serial sections (Figs. 2 and 3). Their differential expression domains as well as their intracellular distributions were summarized below.

TK(+) specific probe

In a frontal section of the E12.5 embryo (Fig. 2A), TK(+) specific signals were not detected in the vicinity of the ventricular zone (VZ) of midbrain and spinal cord, which is totally different from T1 or T2 expression profiles (as described below). TK(+) specific staining instead delineated the ventral mantle zone and subsets of neurons in the dorsal root ganglion (DRG). At the postnatal stages, TK(+) signals were highly detectable in the cerebral cortex (Fig. 3), hippocampus, thalamus and cerebellum (data not shown) as described previously (Dugich-Djordjevic et al., 1993). The signal level at P7 was higher than that at 8W, which is consistent with earlier descriptions (Fryer et al., 1996). At the cellular level, ISH staining signals were always found within the peri-nuclear/cytoplasmic compartment at all stages examined, indicating that these signals are all derived from mature mRNAs.

T1 specific probe

T1 specific signal was distributed in the ventral ventricular side of the midbrain at E12.5 (Fig. 2A). In the rest part of the central nervous system at this developmental stage, the whole VZ was intensely stained by T1 probe. In addition, we found conspicuous stainings at the roof plate (RP) of the spinal cord and emigrating neural crest cells from the RP (Fig. 2B). Nerve associated cells and DRG satellite cells were also demarcated by T1 expression at E12.5. At the postnatal stages, T1 mRNA was strongly expressed in the ependymal cells of all the brain ventricles (Fig. 3 and data not shown) (Dugich-Djordjevic et al., 1993). Noticeable was the fact that intracellular distribution of T1 signal in the ependymal cell population was cytoplasmic and appeared to be actively concentrated at the ventricular side. The T1 specific signals also distributed diffusely in the cerebral cortex, Purkinje cell layer and granule cell layer of cerebellum at adult stage (data not shown), which may reflect T1 expressions in astrocytes (Ohira et al., 2007). T1 expression level was developmentally increased in the cortex and cerebellum as described previously (Fryer et al., 1996).

T2 specific and intron probes

T2 specific probe detected strong signals in the VZ of the midbrain with their staining being localized around the peri-nuclei and T2 showed distinct expression patterns at E12.5 (Fig. 2A, shown with black stars and triangles): Comparing with T1 distribution, T2 was uniquely distributed in the medial mantle zone of the midbrain (Fig. 2A). On the other hand, the intron probes stained similar regions detected with T2 probe but the staining level was weaker than T2 one at E12.5 (Fig. 2A, depicted with black, gray and white triangles). At P7, signal distribution patterns and intensities obtained from the T2 probe became equal to those from probes a and b. Intracellular distributions of these signals were found in the nuclei or at the nuclear membranes around the VZ (Fig. 3A) and cerebellum (data not shown), indicating that these are not all derived from mature mRNAs. At 8W no labeling was detected around the VZ (Fig. 3B) with T2 probe, probes a and b, while they yielded similar signal intensities and intracellular distributions in the adult cerebellum (data not shown). Sense probes for T2, regions a and b did not give any specific signals at all the stages and tissues tested (data not shown). These results suggest that the T2 territory codes one of TrkB isoforms with relevant functions in the expressed areas at E12.5, while the territory only remains to be a part of premature mRNA/intron for other TrkB isoforms at the postnatal stages.

BDNF specific probe

BDNF mRNA was strongly expressed in the trunk epidermis (Fig. 2A) and cranial spiral ganglia (data not shown) at E12.5. At P7, BDNF signal was detected in the CA3 of the hippocampus, mammillary nuclei and other regions previously reported (data not shown). We also confirmed the intense ISH signals in the CA3 and dentate gyrus of the hippocampus and piriform cortex at 8W (Conner et al., 1997). Moderate level of BDNF expression was further observed in the CA1 of the hippocampus, cortex and granule cell layer of the cerebellum at this stage (data not shown) as was described previously. At the cellular level, almost all signals were found distributed to cytoplasmic compartments (data not shown).

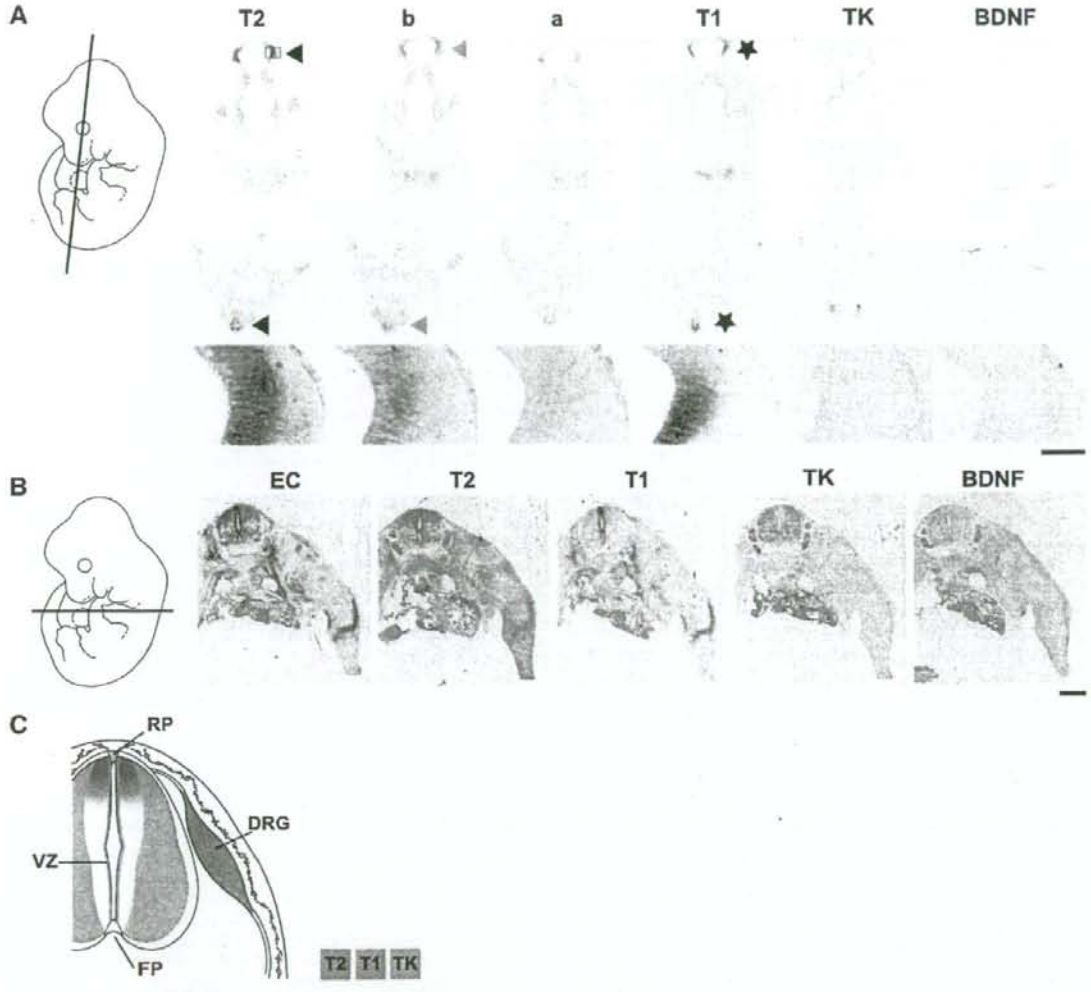

Fig. 2. Dynamic regulation of *Ntrk2* gene expression in the mouse nervous systems at embryonic day (E) 12.5. (A) The upper panels; ISH staining results from mouse E12.5 embryo frontal serial sections are arranged. The section plane is indicated by a line in a schematic drawing of the E12.5 embryo and probes applied are specified above. The lower panels show a high magnification of the boxed area in the upper panels. Note that probes a and b yield only weak stainings compared to specific signals from T2 probe as depicted by triangles (black ones, intense expression; gray ones, intermediate level of expression; white ones, weak expression). T1 probe also stained different regions compared with T2 positive domains. (as shown by stars). Bar indicates 1 mm and 50 μm for the upper and lower panels, respectively. (B) Coronal sections of an E12.5 embryo containing the neural tube are serially collected and processed by ISH, whose results are arranged in the panels. The section plane is indicated by a line in a schematic drawing of the E12.5 embryo and probes used are specified above. Note that T2, T1 and TK signals have different distributions around the ventricular zone. Bar, 500 μm. (C) Summary of T2, T1 and TK(+) expressions in the E12.5 nervous system. Expression domains for T2, T1 and TK(+) are painted with blue, green and pink respectively. T1 signals are distributed in the ventricular cells of the neural tube, roof plate (RP) and migrating neural crest cells. T2 signals delineate the dorsal side of the ventricular zone (VZ) and cells in the dorsal root ganglia (DRG). TK signals demarcate the lateral side of the VZ and only subsets of neurons in the DRG. FP, floor plate.

Comparison of TrkB isoforms and BDNF expressions in the spinal cord at E12.5

As described above, TrkB isoforms appear to differentially demarcate cell populations around the spinal cord at E12.5. To compare TK, T1 and T2 expression patterns more precisely, we performed ISH on serial coronal sections of the spinal cord at E12.5 (Fig. 2B). Consequently, we found that T1 signals were dominantly distributed to the ventricular cells of the neural tube, roof plate and migrating neural crest cells. T2 signals delineated the dorsal side of the VZ and almost all cells in the DRG. TK signals demarcated the lateral side of the VZ and only subsets of neurons in the DRG. These expression domains of TrkB isoforms around the neural tube were illustrated in Fig. 2, highlighting differential expression and roles.

Collectively, we suggest that T2 territory is processed to mRNA encoding a TrkB isoform only at E12.5 but T2 becomes a part of the intron at the postnatal stages. The hypothetical mechanisms of T1 and T2 transcript synthesis are shown in Fig. 3C (see details in Discussions), and that *Ntrk2* gene transcriptional mechanism may be dynamically changed before and after birth.

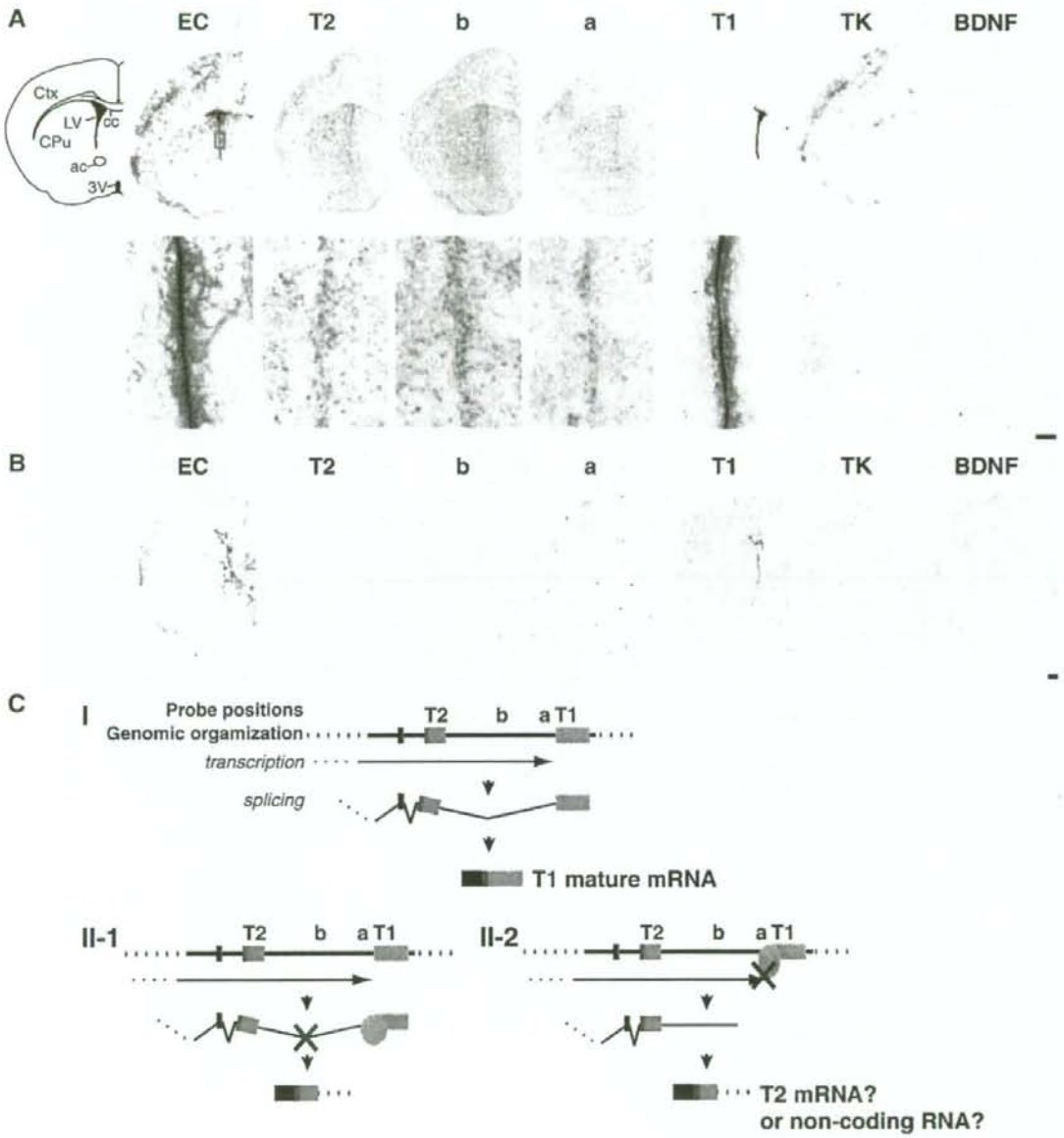

Fig. 3. Dynamic regulation of *Ntrk2* gene expression in the ventricular zone at postnatal stages. (A) The upper panels represent staining results of postnatal day-7 (P7) mouse frontal brain sections with a low magnification. The section appearance is indicated by a schematic drawing. ac, anterior commissure; cc, corpus callosum; CPu, caudate putamen; Ctx, cortex; LV, lateral ventricle; 3V, 3rd ventricle. The lower panels show a high magnification of the boxed area in the upper panels. Staining signals by T2, probe b and a distribute at the nuclear membrane with the identical pattern and intensity. Bar represents 500 μm and 50 μm for the upper and lower panels, respectively. (B) Panels represent results of 8-week-old mouse brain ISH with indicated probes. Note that signals are not detected by probes T2, b and a. Bar, 500 μm. (C) Hypothetical mechanisms of alternative T1 and T2 mRNA synthesis. I. The intron including probe regions T2, b and a is spliced out, and mature T1 mRNA is synthesized. This mechanism is dominantly activated in T1 expressing regions. T2 mRNA or non-coding RNAs are synthesized because a splicing blocker binds to the premature T1 mRNA (II-1) or a transcriptional blocker binds to the 5′-flanking region of T1 exon (II-2). At E12.5 the mechanism II is in action for T2 positive regions by ISH and the mechanism I is applicable to T1 expressing regions, while at postnatal stages only mechanism I is activated.

The 3′-flanking genomic segment of TrkB-TM/JM-T2 exon was dynamically transcribed in the mouse nervous system

To further clarify the transcriptional mechanisms of mouse *Ntrk2* gene locus, we focused on the 3′-flanking region of TrkB-TM/JM-T2 exon and prepared specific probes for six genomic segments, namely regions c, d, e, f, g and h. We then rigorously examined the expression profiles by means of ISH at E12.5 and P7 stages (Fig. 4). Relative positions for these segments were drawn in Figs. 1 and 6 with their sense and antisense orientations being defined along the *Ntrk2* gene/

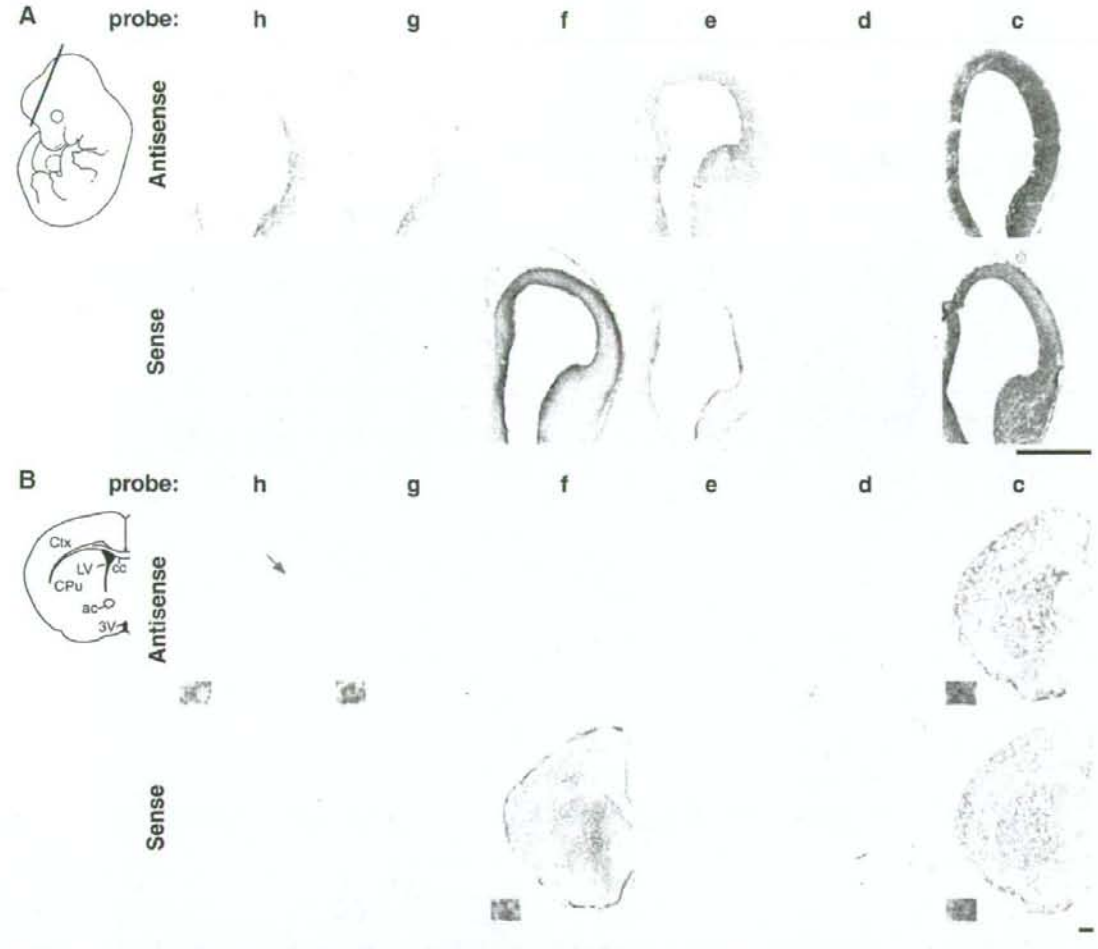

Fig. 4. Multiple territories in the 3'-flanking region of T2 specific exon in the *Ntrk2* gene locus is differentially expressed in the nervous systems. (A) The panels represent ISH results of mouse embryo at E12.5. Probe regions are summarized in Figs. 1 and 6. The upper panels represent staining results with h, g, f, e, d and c antisense probes (AS). The lower panels show staining patterns with their sense probes (S). The section plane is indicated by a line in a schematic drawing of the E12.5 embryo. Bar, 500 μm. (B) The panels represent ISH results of coronal brain sections at P7. The upper panels represent staining results with h, g, f, e, d and c antisense probes (AS). The lower panels show staining patterns with these sense counterparts (S). The section appearance is indicated by a schematic drawing. The inset of each panel shows a high magnification around the ventricular zone pointed by the orange arrow. Note that AS-probes for h, g and d and S-probe for f yield signals however opposite probes have no staining. AS- and S-probe c generate intense signals. Bar signifies 400 μm for the brain sections and 15 μm for the insets. ac, anterior commissure; cc, corpus callosum; CPu, caudate putamen; Ctx, cortex; LV, lateral ventricle; 3V, 3rd ventricle.

TrkB protein coding direction. As was summarized below, their transcriptional directions and expression domains were extremely intricate during brain development, although these six segments are confined within a 7 kb genomic territory.

Probes for region g and h

Regions g and h appeared to yield similar expression profiles at E12.5 and P7. Their antisense (AS)-probes were mainly detected in the ventral side of midbrain VZ (Fig. 4A), prospective cerebral cortex and cochlear nucleus (data not shown) at E12.5. Their signals were intense and showed perinuclear foci at the cell level. As contrasted with the AS-probes, their sense (S)-probes did not detect any expression at E12.5. In P7 brain sections, the AS-probe signals were distributed around the VZ of lateral ventricle (Fig. 4B insets), cerebral cortex (Fig. 4B) and cerebellum (not shown) yet the S-probes did not yield any staining signals. Considering the relative positions in the genome, these two regions may generate a continuous transcript.

Probes for region f

From this genomic segment, the S-probe but not the AS-probe detected RNA expression at E12.5 and P7. The S-probe signals were intense at both the ventricular and marginal zones of the telencephalic

Fig. 5. Nucleotide sequences and deduced amino acid sequences of two novel splicing variants. (A) Two novel splicing variants (T3 alpha and beta) are identified by RT-PCR. The cDNA sequences and deduced amino acid (a.a.) sequences are shown. The predicted transmembrane a.a. sequences are underlined. Novel TrkB-specific a.a. sequences are enclosed by purple boxes. (B) The putative protein structure of new TrkB splicing variants are aligned with those of TK, T1 and T2.

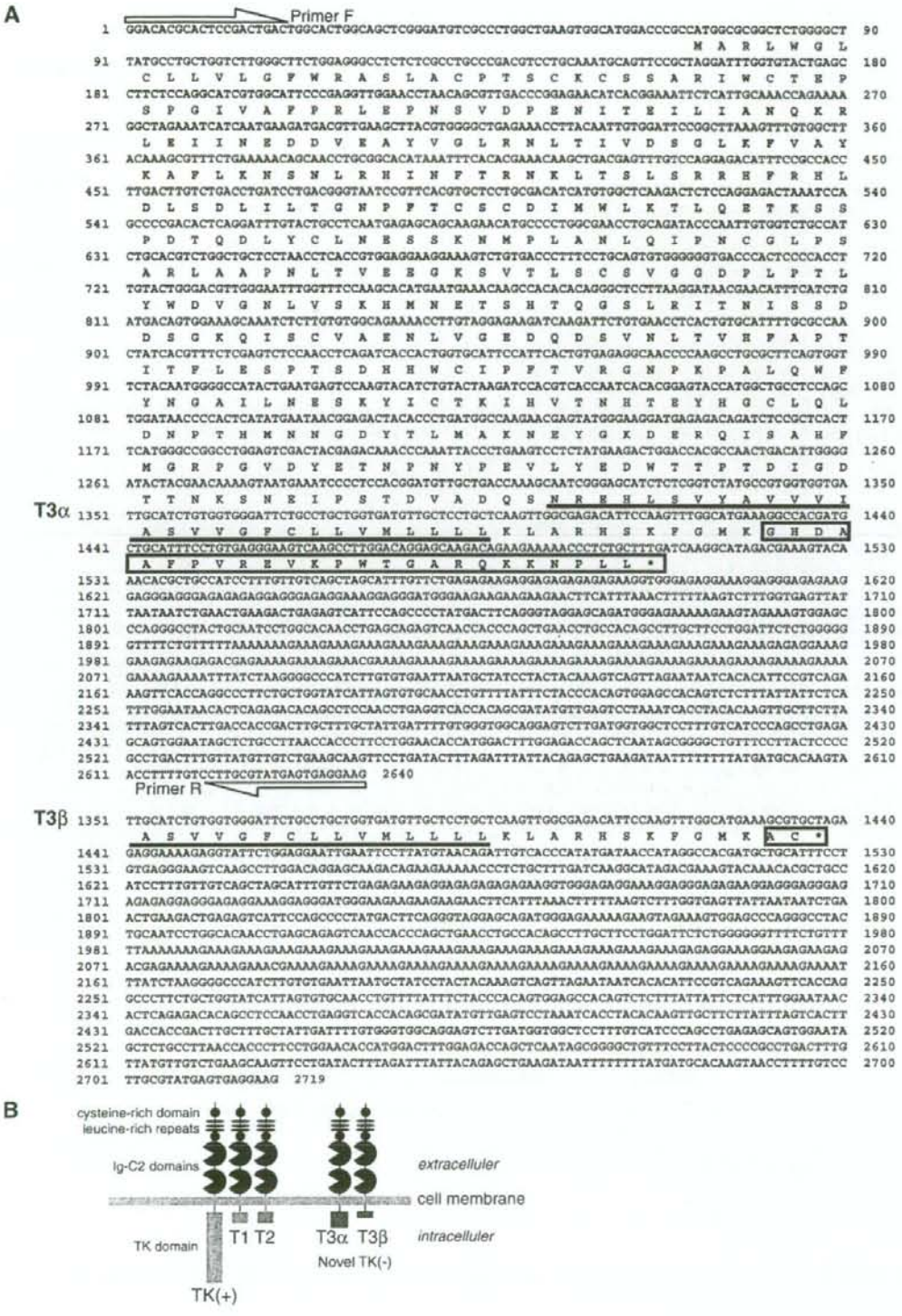
A
Primer F
T3α
T3β
Primer R
B
cysteine-rich domain
leucine-rich repeats
Ig-C2 domains
extracelluler
cell membrane
TK domain
T1 T2
T3α T3β
intracelluler
Novel TK(-)
TK(+)

vesicle (Fig. 4A) at the embryonic stage. At P7, the S-probe signals were strongly detected only at the marginal zone of cerebral cortex (Fig. 4B). The pia mater was also marked by the S-probe. Their intracellular signals were all in the nuclei, indicating these signal are not derived from mature types of mRNA.

Probes for region e

Both chains of this genomic segment were expressed at E12.5, but their expression patterns were diverse. The AS-probe signals were intensely detected at the ventral ventricular side, which is very similar to the staining patterns obtained by the AS-probes g and h. The S-probe yielded the expression profiles resembled with those detected by the aforementioned S-probe f (Fig. 4A). At P7 no signal was observed in the brain by both probes (Fig. 4B), implicating developmental stage specific activation of this genomic segment.

Probes for region d

The AS-probe detected faint signals in the ventral ventricular side of the telencephalic VZ at E12.5 and the distribution patterns were just like those obtained by the AS-probes g, h and e, while the S-probe did not detected any evident signals at this stage (Fig. 4A). At P7, the AS-probe yielded weak signals around the VZ, while the S-probe did not detect any staining signals (Fig. 4B).

Probes for region c

Both the S- and AS-probe detected extremely intense signals, marking a broad variety of cells in the nervous system. In the E12.5 telencephalic vesicles, the AS-probe strongly stained almost all cell populations including the VZ, while the S-probe gave a negative area at around the ventral mantle zone (Fig. 4A). At the cellular level, almost all signals were distributed in the cytoplasm. In some regions, the S-probe signals were detected in the nuclei at the embryonic stage, while the AS-probe signals were found in the cytoplasm. The bidirectional transcription was also observed widely at P7 and all of their intracellular distributions were in nuclei. One clear difference among their expression patterns was found in the ependymal cell layers of the lateral ventricle where only the AS-probe yielded strong staining signals (Fig. 4B).

In summary, although T2 and regions c, d, e, f g, and h were positioned within a 10 kb genomic region, their expression patterns and timing, intracellular distributions and transcriptional direction were extremely variable. These results indicate that the expression of these regions in *Ntrk2* gene locus is strictly regulated and each transcript could harbor important roles.

Identification of novel alternative splicing variants encoding truncated isoforms for TrkB receptor

Since intense ISH signals were detected with probes from region c both at E12.5 and P7, we assumed that the sense transcript from region c is a part of unknown alternative splicing variants of TrkB. We first examined whether cDNA that contains both sequences from the TrkB constitutive exons and region e, d, or c is present. We attempted to amplify such transcripts from the cerebral cortex, cerebellum or liver cDNAs at P7 by means of RT-PCR. For the primer, we designed three forward primers positioned in the TrkB constitutive exons (F1, F2 and F3 in Fig. 6) and reverse primers match to region e, d, and c (R1, R2, R3 and R4 in Fig. 6) or the 5′ flanking region of the 3′-proximal polyadenylation signal sequence from region c (Primer R in Fig. 6). As expected, prominent products were amplified from the cerebral cortex or cerebellum cDNA when we used the reverse primers within region c (R3 or R4) or Primer R. Lengths of these PCR products changed according to positions of the forward primer and were clearly shorter than those of genomic fragment, indicating some introns exist in the genomic region between the TM–JM exon and Primer R (data not shown). We next tried to identify splicing sites in the genomic region. To this end, one PCR product highly amplified by one of the forward primers, F1 and Primer R was cloned into pGEM-T Easy vector and fourteen clones obtained were sequenced with the forward primer F3 located in the TM–JM exon. Consequently, we found that these clones could be divided into two groups by means of their splicing pattern (Figs. 5 and 6): Eleven of these had T3 alpha-type splicing, and the remainder had T3 beta-type splicing. We then re-amplified their full-length cDNAs by the forward primer positioned at the 5′-side of the initiation codon (Primer F) and Primer R and cloned them into the vector. Sequences of their cDNA and deduced amino acids, summarized in Fig. 5, suggested that the cDNA could encode novel types of TrkB-TK(−) receptors. These sequence data have been submitted to the DDBJ databases under accession No. AB377224 for T3 alpha and AB377225 for T3 beta. Briefly, TrkB-T3 alpha variant had 24 specific amino acids in cytoplasmic tail, while TrkB-T3 beta isoform harbored specific tail with two amino acids. Incidentally, T3 alpha specific tail was not conserved among species just as the putative T2 specific cytoplasmic tail, whereas the short T3 beta tail was well conserved

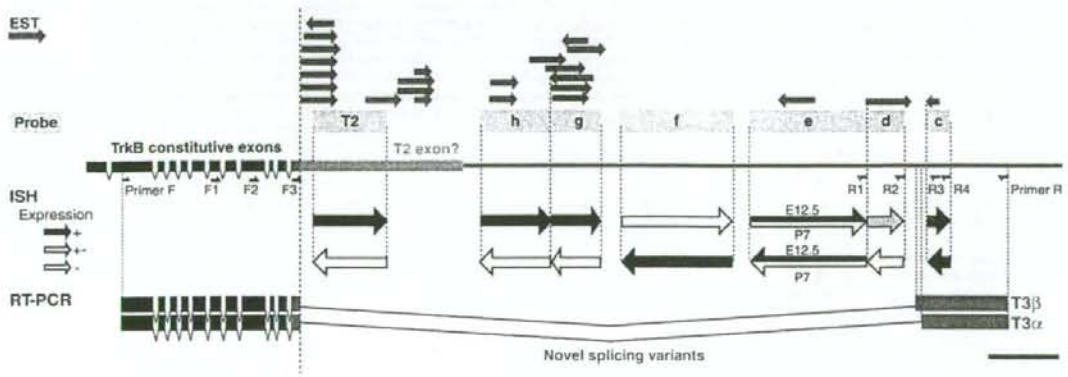

Fig. 6. Summary of transcripts from the 3′-flanking region of T2. In the upper part of the figure, mouse ESTs in the UCSC database are shown by red arrows and probes for ISH are specified by orange boxes. The constitutive exons are indicated by black boxes and the 3′-flanking genomic region of the last constitutive exon is depicted by a bold line with the putative T2 exon colored by light blue, and primers used in this study are depicted. The middle part outlines ISH results by bold arrows and their colors indicate signal intensity; intense (black), weak (gray), none (white). New splicing variants confirmed by our RT-PCR are summarized in the lower part of the figure. Note that those territories annotated by ESTs coincide with the transcribed genomic regions. Bar, 1 kb.

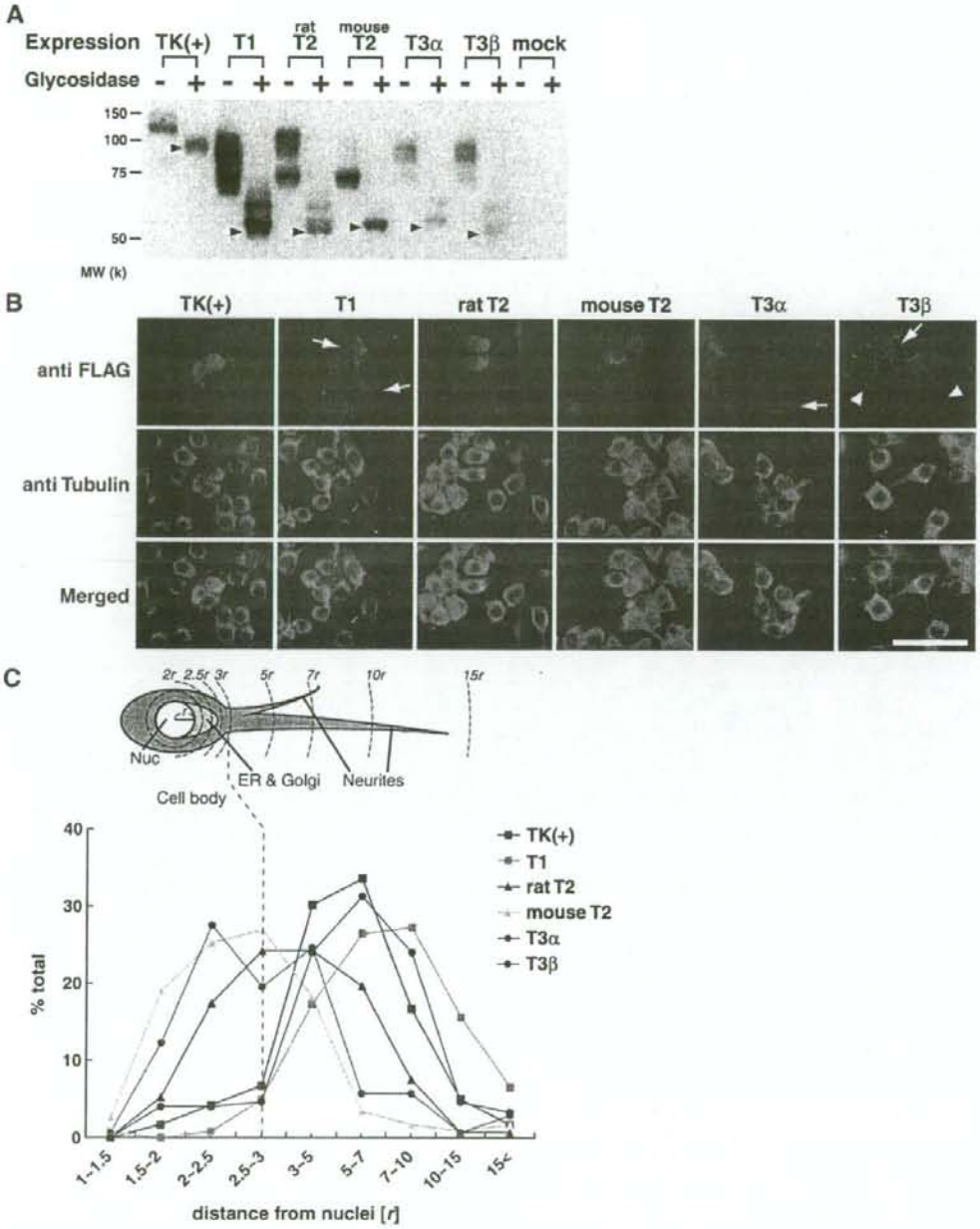

Fig. 7. Different effects from expressed TrkB variants in Neuro-2a neuroblastoma cells. (A) Western blot analysis of FLAG-tagged TrkB variants in Neuro-2a cells. Cell lysates are incubated with (+) or without (−) *N*-Glycosidase F and equal volume of those samples are analyzed by immunoblot with anti-FLAG polyclonal antibody. The apparent molecular weights of deglycosidated TrkB variants are almost identical with the predictive ones (arrowheads). Mock, transfection with expression vector alone. (B) Intracellular distribution of FLAG-tagged TrkB variants in Neuro-2a cells. Cells transfected with FLAG-tagged TrkB variant constructs are immunostained with anti-FLAG antibody (red) and anti-Tubulin antibody (green). Arrows and arrowheads indicate typical distribution patterns and/or effects of each isoform (see Results section). Bar, 50 μm. (C) Each expressed TrkB variant exhibits characteristic response in Neuro2a cells. The upper scheme shows the morphological model of a cell where the radius of the nuclear structure is defined as *r*. We measured the maximum distance from the center of nucleus to the cellular edge among hundreds of parental cells to find the cell body is always included within the circular area with the radius being 3*r* (showed by the broken line spanning the panels) and all the neurite extensions occurring outside of the 3*r* area. Nuc: nucleus, ER & Golgi: endoplasmic reticulum and Golgi apparatus (orange color). The lower graph shows how TrkB variants are expressed by analyzing the distribution pattern along the cellular/neurite extensions. Note that each variant yields a unique graph pattern. The vertical axis, percentages of cell number within the defined circular area; the horizontal axis, distances from the center of cell nuclei measured by *r*.

among mouse, human and dog genomic sequences from the UCSC database (data not shown).

Strict expression and response of TrkB variants in Neuro-2a neuroblastoma

To examine whether the various TrkB transcripts including rat/mouse T2 and novel mouse T3 alpha/beta isoforms encode functional proteins, we sought to transfect their cDNAs into the cultured cells to harbor the FLAG tag at the N-terminus of mature proteins if expressed. To avoid the influence of intact TrkB protein, we adopted Neuro-2a cells which do not express endogenous TrkB (Haapasalo et al., 1999).

At first, we analyzed the expressed TrkB proteins with western blotting. One day after transfection with those tagged constructs, cell lysates were prepared and treated with *N*-Glycosidase F to identify the precise molecular weights of glycosilated TrkB proteins. Consequently, all TrkB variants transfected were found to be detectable with anti-FLAG antibody (Fig. 7A) or anti-TrkB antibody (data not shown) and their apparent molecular weights were identical with their calculated ones (92.1, 53.2, 53.0, 54.5, 54.7 and 52.1 k for TK(+), T1, rat T2, mouse T2, T3 alpha and beta; Arrowheads of Glycosidase+ lanes in Fig. 7A). Thus, TrkB variants were confirmed to be accurately expressed in Neuro-2a cells.

Next, we analyzed the intracellular distribution of TrkB isoforms by anti-FLAG antibody, where anti-Tubulin antibody was simultaneously utilized to visualize the morphology of transfectants (Fig. 7B). As the results, we found that each isoform was differently distributed in the transfectant. To further evaluate those differences in details, we measured the distance from the center of nuclear structure to the most distal staining signal of anti-FLAG antibody in each cell. More than 100 transfectants per one isoform were analyzed and categorized as shown in the upper drawing of Fig. 7C (see details in Experimental methods). As a consequence, we noticed that TK(+) distributed along the neurites (the distance over 3*r*; ~90%). Regarding the T1-isoform, almost all proteins were transported to the distal processes (the distance over 3*r*; ~90%, Fig. 7C) and T1-expressing cells more or less changed their morphology to increase the number of filopodia and processes, sometimes flattening the whole shape (Fig. 7B, arrow), which is consistent with earlier studies (Haapasalo et al., 1999; Hartmann et al., 2004). In contrast, rat and mouse T2 isoforms were mainly distributed to the cell body and proximal neurites without morphological changes (the distance under 5*r*; ~70% for rat T2, ~90% for mouse T2). One of the novel splicing variants, T3 alpha was accumulated at the peri-nuclear structures including the Golgi apparatus in ~40% of the cells (Figs. 7A; arrow, and C; the distance under 2.5*r*), while another ~40% of cells harbored this expressed isoform along the neurites longer than 3*r*, resulting in an M-shaped graph by our analysis (Fig. 7C). T3 beta was transported into the neurites (the distance over 3*r*; ~90%) and the protein distribution pattern analyzed in Fig. 7C was similar to the case of TK(+) at a glance. However, T3 beta-expressing cells displayed flat-shape and increased processes, which rather resembles the case of T1 (Fig. 7B, arrow). T3 beta positive neurites occasionally surrounded the neighboring cells, which is very characteristic to this isoform (Fig. 7B, arrowhead). Taken together, each TrkB isoform was uniquely distributed in a cell and some of variants, T1 and T3 beta, altered the host cell shapes, suggesting that TrkB splicing variants with specific expression profiles may have distinct functions in the developing nervous system.

Discussions

In the present study, we have shown that TrkB isoforms and BDNF are dynamically and differentially expressed in the developing mouse nervous system. Especially, we have demonstrated the possibility that the TrkB-T2 segment is expressed as mRNA at E12.5 yet becomes a part of intron after birth. In addition, we found that mouse *Ntrk2* gene locus is actively regulated to generate multiple transcripts, two of which could encode novel TrkB-TK(−) splicing variants. These results implicate complex ways of splicing and separable functions of mouse *Ntrk2* gene in the nervous system.

Balanced ways of splicing to generate TrkB-TK(+), T1 and T2 isoforms from the mouse Ntrk2 gene locus

We have demonstrated that expression domains of TrkB-TK(+), T1 and T2 are distinct with minimum overlaps in the nervous system and that ISH signals obtained from antisense probes for T2 specific segment are totally dissimilar to those for the continuous intronic segments at the embryonic stage. On the other hand, at the postnatal stages, probes from T2 specific segment and continuous intronic segments all yield similar levels and patterns of ISH staining with maximum overlaps in the nervous system. At the cellular level, distribution and intensity of T2 specific signals are almost equal to those obtained from the intronic probes and all their staining signals were not found in the cytoplasm. These results suggest that T2 specific segment is transcribed as mRNA at the embryonic stages and becomes a part of premature mRNA for other TrkB isoforms at the postnatal stages. How can these spatiotemporally regulated expressions from the *Ntrk2* gene locus be achieved?

We hypothesize balanced regulatory mechanisms in synthesizing T1/TK(+) and T2 transcripts from *Ntrk2* gene locus as is summarized in Fig. 3C: Within those cells specifically express TrkB-T1 or -TK(+), T1 and/or TK(+) mRNAs are dominantly synthesized by splicing out the intron that includes the T2 coding region as is shown in Fig. 3CI. Transcripts including the T2 coding region, regions b and a therefore stand as premature T1 and/or TK(+) mRNAs to be localized in cell nuclei or bind to the nuclear membrane. Within those cells strongly express TrkB-T2 mRNA, transcripts including the T2 coding region become dominant, while T1 and/or TrkB-TK(+) mRNA synthesis is inhibited at the level of splicing (Fig. 3CII-1) or transcription (Fig. 3CII-2). It is still uncertain that transcripts including the T2 coding region are effectively translated into TrkB-T2 protein. Yet if they generate stable protein products, these must exist as one of TrkB isoforms with separable functions other than simple dominant negative molecules to TrkB-T1 and/or -TK(+), since the expression is balanced to produce a defined TrkB isoform in a cell. Whatever the case might be, *Ntrk2* gene transcription mechanism would dynamically change before and after birth. Can this mechanism stand with earlier results?

Armanini et al. have previously shown the expression patterns of TrkB isoforms by ISH using ^{35}S-labeled riboprobes in the E10.5, E13.5 and E15.5 spinal ventral horns and adult hippocampi. Our results are comparable to theirs at the embryonic stages, while we can additionally map the expression profiles with a higher resolution by our sensitive ISH system as illustrated in Fig. 2B, finding out that mouse TrkB-T1 is expressed in the neural crest generating zones (RP) and emigrating subpopulations from the RP. In the adult mouse hippocampi, Armanini et al. have noticed that both TK(+) and T2 specific transcripts are expressed in neuronal cells, yet in our results, T2 signals are not detected in these cell populations at all, while TK(+) and T1 distributions are comparable to theirs (data not shown). Silhol et al. have independently demonstrated that T2 mRNA and its protein product gradually decreased from the postnatal day-7 becoming undetectable by 22-month-old in the rat hippocampus. In light of the non-conserved structure of T2 among species as well as our data demonstrating that mouse T2 may functions as a protein only at embryonic stages, it should rigorously be examined if mouse and/or rat T2 protein is stably expressed in the mature nervous system by using specific antibodies.

Functional significance of multiple transcripts from mouse Ntrk2 gene locus

We found that multiple sense and antisense transcripts are expressed from the 3′-flanking genomic segment of TrkB-TM/JM-T2 exon in *Ntrk2* gene locus as is summarized in Fig. 6. In the present study we could not fully determine whether those transcripts encode protein products or are parts of microRNAs. To investigate *Ntrk2* gene expression mechanism, it would be necessary to identify the full-length of these transcripts.

We have identified two novel transcripts including genomic sequences from region c that encode TrkB-TK(−) splicing variants. We have also demonstrated that ISH signals with the antisense probe for region c are massively distributed in the developing mouse nervous system. Notably, the region c is transcribed from the opposite chain and the ISH signals are equally strong compared to the staining by the antisense probe. It is possible that the antisense transcripts form RNA–RNA duplexes with the novel TrkB transcripts to inhibit translation and/or splicing them as found for the human *BDNF* gene locus (Pruunsild et al., 2007). Hence *bona fide* functional expression domains of the novel TrkB product may be restricted within the antisense product negative areas including the telencephalic mantle zones at E12.5 and ependymal cell layers at P7 (Fig. 4). We have further observed that expressed TrkB isoforms including the novel variant had diverse distribution in Neuro-2a cells. These results indicate that TrkB isoforms have individual functions in their various intracellular locations, elaborating the neural structures at the site of expression *in vivo* (Fig. 7).

Earlier studies have identified some other TrkB variants such as TrkB-T-Shc (Stoilov et al., 2002), a TrkB-TK(+) receptor variant with deletions in the extracellular domain (Ninkina et al., 1997; Strohmaier et al., 1996) and a TrkB-TK(−) with a unique cytoplasmic tail (Garner et al., 1996) in various species. It is further known that both TrkA and TrkC have alternative splicing variants (Barker et al., 1993; Coulier et al., 1990; Esteban et al., 2006; Martin-Zanca et al., 1990), suggesting a common feature of Trk receptor family to create a variety of isoforms for diversifying ligand-binding or signal transduction properties. Considering the evolutional traits (Benito-Gutierrez et al., 2006), our new information might serve as a basis for identifying those elements that balance multiple ways of splicing.

We have observed that BDNF is poorly expressed at E12.5. Are functions of TrkB totally independent of BDNF? The conflict may be explained by their alternative ligands (Reichardt, 2006), such as NT-3 in the trigerminal ganglia (Davies et al., 1995) or by intracellular trafficking and/or broad diffusion of these neurotrophins (Altar and DiStefano, 1998). TrkB could further function as co-receptors for some G-protein coupled receptors or cell adhesion molecules, which is very independent of neurotrophins (Wiese et al., 2007). Such tantalizing scenarios would be subjects for future studies.

In conclusion, our results clearly indicate that TrkB mRNA expressions are strictly regulated at the level of transcription, splicing and/or subcellular localizations. Complex transcriptional regulations of mouse *Ntrk2* gene locus as well as the combinatorial expression profiles and diverse protein functions of each TrkB isoform may support multiple effect of BDNF in the developing nervous system.

Experimental methods

Animals

Time pregnant ICR mice (embryonic 12.5-day-old (E12.5)), postnatal 7-day-old (P7) and 8-week-old (8W) mice were purchased from Clea JAPAN to collect embryos, tissues and RNA samples. The experimental protocol was approved by the Ethics review Committee for Animal Experimentation of National Institute of Neuroscience (NCNP).

In situ hybridization

Preparation of digoxigenin-UTP-labeled RNA probes and *in situ* hybridization (ISH) were performed as described previously with slight modifications (Inoue et al., 1998). PCR was performed to amplify probe fragments of TrkB isoform-specific regions from mouse brain cDNA or those of intron regions from BAC (#RP23-141B16) DNA, and the amplified fragments were cloned into pBluescript II vector (Stratagene, USA). Primers were designed as follows: TrkB extracellular domain (forward, 5′-CATGGATCCTGACCCACTCCCCACCTTG-3′, reverse, 5′-CATAAGCTTCGACTC-CAGGCCGGCCCATG-3′), T1 (forward, 5′-GATCCCACTGGATGGGTAGCTGA-GATAAAG-3′, reverse, 5′-TAATTCAGGTCCATACTCCTGGCCACACAG-3′), T2 (forward, 5′-CTCGCTCGAGGAGATGTGGCCGTCCGGACTCATGAC-3′, reverse, 5′-CATAAGTCGACCCTGCTTTCCAGTGAGCGCGGTTGT-3′), TK (forward, 5′-CGGGGATCCGGTATCACCAACAGCCAGCTCAAGCCG-3′, reverse, 5′-CCCAAGCTTCTCGGTGGGCGGGTTACCCTCTGCCATC-3′), Region a (forward, 5′-CAGACCAGACCTACTCGAGGAAGGCAGAG-3′, reverse, 5′-CACGG-GCATCACGTGACTGAGCAACTTCG-3′), Region b (forward, 5′-GCACAT-CATGCCTTGTGAGCAGA-3′, reverse, 5′-CTTTGCCTTCCTGTTCGAGCTGC-3′), Region c (forward, 5′-GATCAAGGCATAGACGAAAGTAC-3′, reverse, 5′-GTTGACTCTGCTCAGGTTGTGCCAG-3′), Region d (forward, 5′-GTACATG-CACAGAGTGTATATGAC-3′, reverse, 5′-TCCTCCCAGAAGAAGCAGCAAC-3′), Region e (forward, 5′-TGAAGGCAGAGGAGGCTTACGCTGTG-3′, reverse, 5′-CAAGGGGGAAATGCAGAGGCGAAGTC-3′), Region f (forward, 5′-GACAGACAGCATGCTGGAGAAG-3′, reverse, 5′-GTGAGACTGAGATA-GACTCCCG-3′), Region g (forward, 5′-AAAGGCAGTTTTCTCTCACAGC-3′, reverse, 5′-GCTCTGTTCTGGTTATCTACAC-3′), Region h (forward, 5′-CGCTCTTCTAATGTAGGAACTC-3′, reverse 5′-ACTTCTGCCATCTCTTAG-GACC-3′). The probe for BDNF is prepared from the part of the coding region (150–774 nucleotides from ATG initiation codon).

Whole E12.5 embryos and P7 mouse brains were fixed with 4% paraformaldehyde (PFA) in phosphate buffered saline (PBS). 8W mouse brains were fixed by transcardial perfusion with PBS followed by 4% PFA in PBS at 4 °C. The embryos and brains were immersed in the fixative overnight at 4 °C, followed by treatments of a graded series of sucrose solutions (5 10 15 20%) in PBS, embedded in Tissue-Tek optimal cutting temperature (OCT) compound (Sakura Finetek, Japan), and frozen on a block of dry-ice. For E12.5 embryos, 18 μm frontal or coronal sections were serially collected on slide glasses coated by Vectabond Reagent (Vector Laboratories, Burlingame, CA). We further collected 25 μm frontal sections for P7 brains and 14 μm frontal sections for adult brains. To obtain the high sensitive and stringent results, the steps of hybridization and post-hybridization wash were carried out at 65 °C to avoid nonspecific bindings and the detection periods of each antisense and sense probe were always equal by using the high sensitive detection reagent containing polyvinyl alcohol. For ISH experiment in Figs. 2 and 3, ISH was performed with sense probes for EC, T1, T2 and region a and b, and we confirmed that no signal was detected with these sense probes. Stained sections were photographed under bright field system of a Keyence microscope (Biorevo) or a Leica microscope (DM5000B) equipped with a Leica digital camera (FX300).

Cloning of novel TrkB splicing variants by RT-PCR

Total RNA was prepared from P7 mouse cerebral cortices, cerebella and livers using the protocol provided by the manufacturer of TRIzoL reagent (Invitrogen, California, USA) and purified with RNeasy Mini Kit (Qiagen, Germany). One microgram of total RNA was converted into cDNA by reverse transcription (RT) using ReverTra Ace (TOYOBO, Japan) with oligo $d(T)_{12-18}$ primers (Invitrogen). Novel splicing variants were screened by RT-PCR using the following primer pairs; F1, F2 or F3 with R1 for region e, F1, F2, or F3 with R2 for region d, and F1, F2, or F3 with R3 or R4 for region c, as was represented in Figs. 5 and 6. As a negative control, the

template without RT reaction was used and we confirmed that few PCR products were amplified (data not shown). The forward primer and reverse primer sequences were as follows; Forward primers; F1 (5′-GGTCTGCCGTCTGCACGTCTG-3′), F2 (5′-GGTGCATCCCATTCACTGTG-3′), F3 (5′-CTGCTCAAGTTGGCGAGAC-3′), Reverse primers; R1 (5′-CAAGGGGGAAATGCAGAGGCGAAGTC-3′), R2 (5′-TCCTCCCAGAAGAAGCAGCAAC-3′), R3 (5′-GACAACAAAGGATGGCAGCGTG-3′), R4 (5′-GTTGACTCTGCTCAGGTTGTGCCAG-3′). The full-length cDNA of novel TrkB splicing variants was amplified by PCR using KOD plus (TOYOBO, Japan) with Primer F and Primer R represented in Figs. 5 and 6. These RT-PCR products were cloned into pBluescript II vector (Stratagene, USA) and sequenced.

Nucleotide sequence accession numbers

Nucleotide sequence accession numbers assigned by the DDBJ databases are AB377224 for T3 alpha and AB377225 for T3 beta.

Construction of FLAG-tagged TrkB variant expression vectors

TrkB-TK/-T1 isoforms and rat TrkB-T2 cDNA were subcloned into pcDNA3.1(−) expression vector (Invitrogen, Carlsbad, CA) as described previously (Ohira et al., 2005). Regarding mouse TrkB-T2, the cDNA was amplified from mouse embryonic cDNA via PCR with Primer F and the reverse primer positioned at the 3′ flanking sequence of the putative stop codon (5′-GGTTTGCATGGCAACCCCAC-3′) and the PCR product was subcloned into pcDNA3.1(−). TrkB-T3 alpha and beta cDNAs in pBluescript II described above were cut by *Apa*I and *Eco*RI respectively and subcloned into pcDNA3.1(−). As described previously, FLAG tag was inserted into the putative signal peptide cleavage site, which will not interfere with the ability of BDNF binding and autophosphorylation of TrkB-TK(+) (Haapasalo et al., 1999; Kryl et al., 1999).

Cell culture and transfection

Neuro-2a mouse neuroblastoma cells were maintained in Dulbecco's modified Eagle's minimum essential medium supplemented with 10% fatal bovine serum, 100 U/ml penicillin and 100 μg/ml streptomycin in humidified atmosphere containing 5% CO_2 at 37 °C. The cells (1.0×10^5 cells/well) were plated on 12-well plates containing glass coverslips coated with polyethyleneimine (0.1%) the day prior to transfection. TrkB variant constructs (1 μg/well) were introduced into the cells by TransFectin reagent (Bio-Rad, Hercules, CA).

Western blot analysis

Cells were lysed by 0.5% Nonidet P-40 in PBS with protease inhibitors for 15 min at 4 °C. After the lysed cells were centrifuged at 10,000 ×*g* for 15 min at 4 °C, the supernatants were denaturated with SDS-sample buffer and boiled for 3 min. In the case of deglycosilation of TrkB isoforms, the lysates were incubated with 1 U of *N*-glycosidase F (Roche, Indianapolis, IN)) in deglycosilation buffer (0.5% NP-40, 0.1% SDS, 1% 2-mercaptoethanol and 10 mM EDTA in PBS) before denaturating. Samples were subjected to sodium dodecyl sulfate-polyacrylamide gel electrophoresis (10% gel), and the proteins were blotted onto the PVDF membrane (Millipore, Bedford, MA). The blotted membranes were blocked in 5% skimmed milk in PBS. The blots were then incubated with anti-FLAG polyclonal antibody (diluted at 1/500; Sigma, St. Louis, MO) or anti-TrkB polyclonal antibody (diluted at 1/500; Santa Cruz Biotechnology, Santa Cruz, CA) at 4 °C overnight, and washed for 30 min in Tris buffered saline containing 0.05% Tween 20. They were incubated with the secondary antibody conjugated with horseradish peroxidase and the proteins were visualized with Western Lightning enhanced chemiluminescence system (Perkin Elmer, Waltham, MA).

Immunocytochemistry

Cells were fixed for 15 min in PBS containing 4% PFA and permeabilized for 5 min in 0.05% Triton X-100 in PBS. After blocking with 4% goat serum in PBS for 2 h at RT, the cells were incubated overnight at 4 °C with anti-FLAG antibody (diluted at 1/10,000; Sigma) and wash three times with PBS. The cells were then incubated with anti-rabbit IgG-Cy3 (diluted at 1/500; Millipore) with anti-Tubulin-FITC (Sigma) for 3 h at RT. These samples were analyzed using the Leica DM5000B microscope setting.

Analysis of cell morphology

Cells immunostained were randomly chosen and the distance between the center of nuclei and the most distant immunostaining signal from the cell body was measured. We measured 119, 121, 132, 115, 138 and 150 cells for TK(+), T1, rat T2, mouse T2, T3 alpha and T3 beta, respectively. Briefly, captured cell images were superimposed to the concentric circles prepared with Photoshop software with the elemental radius being defined as *r* which is equal to the radius of the nuclear structure. The measurements were then classified into 1*r*–1.5*r*, 1.5*r*–2*r*, 2*r*–2.5*r*, 2.5*r*–3*r*, 3*r*–5*r*, 5*r*–7*r*, 7*r*–10*r*, 10*r*–15*r* and over 15*r*. The percentages of cell number with those categories were calculated and graphed.

Acknowledgments

We thank Drs. Koji Ohira, Masami Kojima, Mikio Hoshino and other members of the Shindan Laboratory for their technical advice and fruitful discussions.

This work was supported by a National Institute of Biomedical Innovation grant (#05-32) to H.K., S.N. and T.I. and a health sciences research grant of nano-1 to S.N.

References

Altar, C.A., DiStefano, P.S., 1998. Neurotrophin trafficking by anterograde transport. Trends. Neurosci. 21, 433–437.
Armanini, M.P., McMahon, S.B., Sutherland, J., Shelton, D.L., Phillips, H.S., 1995. Truncated and catalytic isoforms of trkB are co-expressed in neurons of rat and mouse CNS. Eur. J. Neurosci. 7, 1403–1409.
Barker, P.A., Lomen-Hoerth, C., Gensch, E.M., Meakin, S.O., Glass, D.J., Shooter, E.M., 1993. Tissue-specific alternative splicing generates two isoforms of the trkA receptor. J. Biol. Chem. 268, 15150–15157.
Benito-Gutierrez, E., Garcia-Fernandez, J., Comella, J.X., 2006. Origin and evolution of the Trk family of neurotrophic receptors. Mol. Cell. Neurosci. 31, 179–192.
Bibel, M., Barde, Y.A., 2000. Neurotrophins: key regulators of cell fate and cell shape in the vertebrate nervous system. Genes. Dev. 14, 2919–2937.
Blum, R., Konnerth, A., 2005. Neurotrophin-mediated rapid signaling in the central nervous system: mechanisms and functions. Physiology (Bethesda) 20, 70–78.
Chiaruttini, C., Sonego, M., Baj, G., Simonato, M., Tongiorgi, E., 2008. BDNF mRNA splice variants display activity-dependent targeting to distinct hippocampal laminae. Mol. Cell. Neurosci. 37, 11–19.
Conner, J.M., Lauterborn, J.C., Yan, Q., Gall, C.M., Varon, S., 1997. Distribution of brain-derived neurotrophic factor (BDNF) protein and mRNA in the normal adult rat CNS: evidence for anterograde axonal transport. J. Neurosci. 17, 2295–2313.
Conover, J.C., Erickson, J.T., Katz, D.M., Bianchi, L.M., Poueymirou, W.T., McClain, J., Pan, L., Helgren, M., Ip, N.Y., Boland, P., et al., 1995. Neuronal deficits, not involving motor neurons, in mice lacking BDNF and/or NT4. Nature 375, 235–238.
Coulier, F., Kumar, R., Ernst, M., Klein, R., Martin-Zanca, D., Barbacid, M., 1990. Human trk oncogenes activated by point mutation, in-frame deletion, and duplication of the tyrosine kinase domain. Mol. Cell. Biol. 10, 4202–4210.
Davies, A.M., Minichiello, L., Klein, R., 1995. Developmental changes in NT3 signalling via TrkA and TrkB in embryonic neurons. EMBO J. 14, 4482–4489.
Dugich-Djordjevic, M.M., Ohsawa, F., Hefti, F., 1993. Transient elevation in catalytic trkB mRNA during postnatal development of the rat brain. Neuroreport 4, 1091–1094.
Eide, F.F., Vining, E.R., Eide, B.L., Zang, K., Wang, X.Y., Reichardt, L.F., 1996. Naturally occurring truncated trkB receptors have dominant inhibitory effects on brain-derived neurotrophic factor signaling. J. Neurosci. 16, 3123–3129.

Ernfors, P., Van De Water, T., Loring, J., Jaenisch, R., 1995. Complementary roles of BDNF and NT-3 in vestibular and auditory development. Neuron 14, 1153–1164.
Esteban, P.F., Yoon, H.Y., Becker, J., Dorsey, S.G., Caprari, P., Palko, M.E., Coppola, V., Saragovi, H.U., Randazzo, P.A., Tessarollo, L., 2006. A kinase-deficient TrkC receptor isoform activates Arf6-Rac1 signaling through the scaffold protein tamalin. J. Cell Biol. 173, 291–299.
Fryer, R.H., Kaplan, D.R., Feinstein, S.C., Radeke, M.J., Grayson, D.R., Kromer, L.F., 1996. Developmental and mature expression of full-length and truncated TrkB receptors in the rat forebrain. J. Comp. Neurol. 374, 21–40.
Garner, A.S., Menegay, H.J., Boeshore, K.L., Xie, X.Y., Voci, J.M., Johnson, J.E., Large, T.H., 1996. Expression of TrkB receptor isoforms in the developing avian visual system. J. Neurosci. 16, 1740–1752.
Haapasalo, A., Saarelainen, T., Moshnyakov, M., Arumae, U., Kiema, T.R., Saarma, M., Wong, G., Castren, E., 1999. Expression of the naturally occurring truncated trkB neurotrophin receptor induces outgrowth of filopodia and processes in neuroblastoma cells. Oncogene 18, 1285–1296.
Haapasalo, A., Koponen, E., Hoppe, E., Wong, G., Castren, E., 2001. Truncated trkB.T1 is dominant negative inhibitor of trkB.TK+-mediated cell survival. Biochem. Biophys. Res. Commun. 280, 1352–1358.
Hartmann, M., Brigadski, T., Erdmann, K.S., Holtmann, B., Sendtner, M., Narz, F., Lessmann, V., 2004. Truncated TrkB receptor-induced outgrowth of dendritic filopodia involves the p75 neurotrophin receptor. J. Cell Sci. 117, 5803–5814.
Inoue, T., Tanaka, T., Suzuki, S.C., Takeichi, M., 1998. Cadherin-6 in the developing mouse brain: expression along restricted connection systems and synaptic localization suggest a potential role in neuronal circuitry. Dev. Dyn. 211, 338–351.
Itami, C., Kimura, F., Nakamura, S., 2007. Brain-derived neurotrophic factor regulates the maturation of layer 4 fast-spiking cells after the second postnatal week in the developing barrel cortex. J. Neurosci. 27, 2241–2252.
Jones, K.R., Farinas, I., Backus, C., Reichardt, L.F., 1994. Targeted disruption of the BDNF gene perturbs brain and sensory neuron development but not motor neuron development. Cell 76, 989–999.
Klein, R., Parada, L.F., Coulier, F., Barbacid, M., 1989. trkB, a novel tyrosine protein kinase receptor expressed during mouse neural development. EMBO J. 8, 3701–3709.
Klein, R., Smeyne, R.J., Wurst, W., Long, L.K., Auerbach, B.A., Joyner, A.L., Barbacid, M., 1993. Targeted disruption of the trkB neurotrophin receptor gene results in nervous system lesions and neonatal death. Cell 75, 113–122.
Kryl, D., Yacoubian, T., Haapasalo, A., Castren, E., Lo, D., Barker, P.A., 1999. Subcellular localization of full-length and truncated Trk receptor isoforms in polarized neurons and epithelial cells. J. Neurosci. 19, 5823–5833.
Li, Y.X., Xu, Y., Ju, D., Lester, H.A., Davidson, N., Schuman, E.M., 1998. Expression of a dominant negative TrkB receptor, T1, reveals a requirement for presynaptic signaling in BDNF-induced synaptic potentiation in cultured hippocampal neurons. Proc. Natl. Acad. Sci. U. S. A. 95, 10884–10889.
Liu, X., Ernfors, P., Wu, H., Jaenisch, R., 1995. Sensory but not motor neuron deficits in mice lacking NT4 and BDNF. Nature 375, 238–241.
Luikart, B.W., Nef, S., Shipman, T., Parada, L.F., 2003. In vivo role of truncated trkb receptors during sensory ganglion neurogenesis. Neuroscience 117, 847–858.
Martin-Zanca, D., Barbacid, M., Parada, L.F., 1990. Expression of the trk proto-oncogene is restricted to the sensory cranial and spinal ganglia of neural crest origin in mouse development. Genes. Dev. 4, 683–694.
McMahon, S.B., Armanini, M.P., Ling, L.H., Phillips, H.S., 1994. Expression and coexpression of Trk receptors in subpopulations of adult primary sensory neurons projecting to identified peripheral targets. Neuron 12, 1161–1171.
Middlemas, D.S., Lindberg, R.A., Hunter, T., 1991. trkB, a neural receptor protein-tyrosine kinase: evidence for a full-length and two truncated receptors. Mol. Cell. Biol. 11, 143–153.
Murer, M.G., Yan, Q., Raisman-Vozari, R., 2001. Brain-derived neurotrophic factor in the control human brain, and in Alzheimer's disease and Parkinson's disease. Prog. Neurobiol. 63, 71–124.
Ninkina, N., Grashchuck, M., Buchman, V.L., Davies, A.M., 1997. TrkB variants with deletions in the leucine-rich motifs of the extracellular domain. J. Biol. Chem. 272, 13019–13025.
Ohira, K., Kumanogoh, H., Sahara, Y., Homma, K.J., Hirai, H., Nakamura, S., Hayashi, M., 2005. A truncated tropomyosin-related kinase B receptor, T1, regulates glial cell morphology via Rho GDP dissociation inhibitor 1. J. Neurosci. 25, 1343–1353.
Ohira, K., Funatsu, N., Homma, K.J., Sahara, Y., Hayashi, M., Kaneko, T., Nakamura, S., 2007. Truncated TrkB-T1 regulates the morphology of neocortical layer I astrocytes in adult rat brain slices. Eur. J. Neurosci. 25, 406–416.
Poo, M.M., 2001. Neurotrophins as synaptic modulators. Nat. Rev. Neurosci. 2, 24–32.
Pruunsild, P., Kazantseva, A., Aid, T., Palm, K., Timmusk, T., 2007. Dissecting the human BDNF locus: bidirectional transcription, complex splicing, and multiple promoters. Genomics 90, 397–406.
Reichardt, L.F., 2006. Neurotrophin-regulated signalling pathways. Philos. Trans. R. Soc. Lond. B. Biol. Sci. 361, 1545–1564.
Rose, C.R., Blum, R., Pichler, B., Lepier, A., Kafitz, K.W., Konnerth, A., 2003. Truncated TrkB-T1 mediates neurotrophin-evoked calcium signalling in glia cells. Nature 426, 74–78.
Siegel, G.J., Chauhan, N.B., 2000. Neurotrophic factors in Alzheimer's and Parkinson's disease brain. Brain Res. Brain Res. Rev. 33, 199–227.
Silhol, M., Bonnichon, V., Rage, F., Tapia-Arancibia, L., 2005. Age-related changes in brain-derived neurotrophic factor and tyrosine kinase receptor isoforms in the hippocampus and hypothalamus in male rats. Neuroscience 132, 613–624.
Stoilov, P., Castren, E., Stamm, S., 2002. Analysis of the human TrkB gene genomic organization reveals novel TrkB isoforms, unusual gene length, and splicing mechanism. Biochem. Biophys. Res. Commun. 290, 1054–1065.
Strohmaier, C., Carter, B.D., Urfer, R., Barde, Y.A., Dechant, G., 1996. A splice variant of the neurotrophin receptor trkB with increased specificity for brain-derived neurotrophic factor. EMBO J. 15, 3332–3337.
Wiese, S., Jablonka, S., Holtmann, B., Orel, N., Rajagopal, R., Chao, M.V., Sendtner, M., 2007. Adenosine receptor A2A-R contributes to motoneuron survival by transactivating the tyrosine kinase receptor TrkB. Proc. Natl. Acad. Sci. U. S. A. 104, 17210–17215.
Zuccato, C., Cattaneo, E., 2007. Role of brain-derived neurotrophic factor in Huntington's disease. Prog. Neurobiol. 81, 294–330.

Human Molecular Genetics, 2008, Vol. 17, No. 10 **1482–1496**
doi:10.1093/hmg/ddn037
Advance Access published on February 4, 2008

Aberrant molecular properties shared by familial Parkinson's disease-associated mutant UCH-L1 and carbonyl-modified UCH-L1

Tomohiro Kabuta[1,2,*], Rieko Setsuie[1,2], Takeshi Mitsui[1,3], Aiko Kinugawa[1], Mikako Sakurai[1], Shunsuke Aoki[1], Kenko Uchida[3] and Keiji Wada[1,*]

[1]Department of Degenerative Neurological Diseases, National Institute of Neuroscience, National Center of Neurology and Psychiatry, 4-1-1 Ogawahigashi, Kodaira, Tokyo 187-8502, Japan, [2]The Japan Health Sciences Foundation, 13-4 Nihonbashi Kodenma, Chuo-ku, Tokyo 103-0001, Japan and [3]Department of Electrical Engineering and Bioscience, Waseda University, Tokyo 169-8555, Japan

Received January 8, 2008; Revised and Accepted January 30, 2008

Parkinson's disease (PD) is a neurodegenerative disorder characterized by loss of dopaminergic neurons. The I93M mutation in ubiquitin C-terminal hydrolase L1 (UCH-L1) is associated with familial PD, and we have previously shown that the I93M UCH-L1-transgenic mice exhibit dopaminergic cell loss. Over 90% of neurodegenerative diseases, including PD, occur sporadically. However, the molecular mechanisms underlying sporadic PD as well as PD associated with I93M UCH-L1 are largely unknown. UCH-L1 is abundant (1–5% of total soluble protein) in the brain and is a major target of oxidative/carbonyl damage associated with sporadic PD. As well, abnormal microtubule dynamics and tubulin polymerization are associated with several neurodegenerative diseases including frontotemporal dementia and parkinsonism linked to chromosome 17. Here we show that familial PD-associated mutant UCH-L1 and carbonyl-modified UCH-L1 display shared aberrant properties: compared with wild-type UCH-L1, they exhibit increased insolubility and elevated interactions with multiple proteins, which are characteristics of several neurodegenerative diseases-linked mutants. Circular dichroism analyses suggest similar structural changes in both UCH-L1 variants. We further report that one of the proteins interacting with UCH-L1 is tubulin, and that aberrant interaction of mutant or carbonyl-modified UCH-L1 with tubulin modulates tubulin polymerization. These findings may underlie the toxic gain of function by mutant UCH-L1 in familial PD. Our results also suggest that the carbonyl modification of UCH-L1 and subsequent abnormal interactions of carbonyl-modified UCH-L1 with multiple proteins, including tubulin, constitute one of the causes of sporadic PD.

INTRODUCTION

Parkinson's disease (PD) is the most common neurodegenerative movement disorder and is characterized by progressive cell loss confined mostly to dopaminergic neurons in the substantia nigra pars compacta. The I93M mutation in ubiquitin C-terminal hydrolase L1 (UCH-L1) was reported in a German family with dominantly inherited PD (1). To assess the correlation of the I93M mutation and pathogenesis of PD, we have previously generated UCH-L1^{I93M}-transgenic mice. These mice exhibited progressive dopaminergic cell loss in the substantia nigra (2), suggesting that the I93M mutation in UCH-L1 is a causative mutation for PD. The S18Y polymorphism in UCH-L1 has been reported to be associated with decreased risk of PD (3). However, it has also been reported that S18Y is not associated with risk of PD (4).

UCH-L1 is abundant (1–5% of total soluble protein) in the brain (5) and is thought to hydrolyse polymeric ubiquitin and ubiquitin conjugates to monoubiquitin (6). UCH-L1 has also been reported to act as a ubiquitin ligase *in vitro* (7). In

*To whom correspondence should be addressed. Tel: +81 423461715; Fax: +81 423461745; Email: kabuta@ncnp.go.jp (T.K.); wada@ncnp.go.jp (K.W.)

addition to these enzymatic activities, we have found that UCH-L1 binds to and stabilizes monoubiquitin in neurons (8). Our previous studies using circular dichroism (CD) and small-angle neutron scattering strongly suggested that the I93M mutation in UCH-L1 alters the conformation of UCH-L1 (9,10). We have previously shown that mice deficient in UCH-L1 do not exhibit obvious dopaminergic cell loss, in contrast to UCH-L1^{I93M}-transgenic mice (2,8,11), suggesting that a loss or decrease in the level of UCH-L1 is not the main cause of PD, and that UCH-L1^{I93M}-associated PD is caused by an acquired toxicity. Thus, although the hydrolase activity of UCH-L1^{I93M} is decreased (1,9), this decreased activity may not be a major cause of PD.

Increased oxidative stress is associated with neurodegenerative diseases (12,13). In sporadic PD brains, UCH-L1 is a major target of carbonyl formation (12), which is the most widely used marker for oxidative damage to proteins. UCH-L1 has also been identified as a component of several inclusion bodies characteristic of neurodegenerative diseases, including Lewy bodies (14). These findings suggest that UCH-L1 and its modification by carbonyl formation are involved in the cause of sporadic PD. Despite the fact that the majority of PD cases occur sporadically, the molecular mechanisms underlying the causes of sporadic PD, as well as UCH-L1^{I93M}-associated PD, are largely unknown. Moreover, the biochemical properties of UCH-L1^{I93M} and carbonyl-modified UCH-L1 in mammalian cells, such as their protein interactions or detergent insolubility (i.e. the amount of a protein in the insoluble fraction), are poorly understood.

In this study, we analyzed the molecular properties of carbonyl-modified UCH-L1 and UCH-L1^{I93M} and elucidated novel properties of UCH-L1 variants, including protein interactions. We show that carbonyl-modified UCH-L1 and UCH-L1^{I93M} share common properties. Our findings provide novel insights into understanding the mechanisms underlying the toxic gain of function by mutant UCH-L1 and suggest that oxidative stress and subsequent protein interactions of carbonyl-modified UCH-L1 constitute one of the causes of sporadic PD. We also discuss the possible involvement of oxidative modifications of UCH-L1 in other neurodegenerative diseases.

RESULTS

Disease-associated mutants including UCH-L1^{I93M} display aberrant insolubility

Aberrantly increased insolubility compared with wild-type protein is a common biochemical feature of several mutant proteins associated with neurodegenerative diseases: for example, mutant α-synuclein associated with familial PD (15), mutant SOD1 associated with familial amyotrophic lateral sclerosis (ALS) (16,17) and mutant tau associated with frontotemporal dementia and parkinsonism linked to chromosome 17 (18). Although we have previously shown that the insolubility of UCH-L1 in the UCH-L1^{I93M}-transgenic mouse brain is increased compared with that in wild-type mouse (2), the insolubility of UCH-L1^{I93M} itself has been unclear. We observed that pathogenic α-synuclein and SOD1 mutant proteins exhibit increased detergent insolubility in mammalian cells compared with wild-type proteins (Fig. 1A and B). The insolubility of UCH-L1^{I93M} was examined under the same experimental conditions, in which the causative mutants are distinguishable from wild-type proteins. We found that, in dopaminergic SH-SY5Y cells, the protein level of UCH-L1^{I93M} in the insoluble fraction was markedly higher than the levels of UCH-L1^{WT}, UCH-L1^{S18Y}, UCH-L1^{D30K}, which lacks hydrolase activity and binding affinity for ubiquitin (8), and UCH-L1^{C90S}, which lacks hydrolase activity but maintains binding affinity for ubiquitin (8) (Fig. 1C). There was no notable difference among the soluble protein levels (Fig. 1C). The formation of high molecular weight aggregates, which is also a common feature of several mutants, was observed almost exclusively in the insoluble fraction with UCH-L1^{I93M} (Fig. 1C), consistent with the report that UCH-L1^{I93M} produced more aggresomes than UCH-L1^{WT} (19). Increased insolubility of UCH-L1^{I93M} and UCH-L1$^{S18Y/I93M}$ and an increase in the amounts of aggregates specific for these proteins were observed in COS-7 cells (Fig. 1D; Supplementary Material, Fig. S1A), which express very low levels of endogenous UCH-L1. These results demonstrate that UCH-L1^{I93M} shares common features with several mutant proteins linked to neurodegenerative diseases, thus, further supporting the idea that the I93M mutation in UCH-L1 is a causative mutation for PD. Our results also suggest that the insolubility of UCH-L1 is independent of monoubiquitin-binding.

UCH-L1^{I93M} abnormally interacts with multiple proteins

Although increased insolubility is a common characteristic of several mutant proteins associated with neurodegenerative diseases, and this may play a role in the neurotoxicity of the mutant proteins, accumulating evidence suggests that a soluble mutant is the main cause of neurodegeneration (20,21). Studies of dominantly inherited neurodegenerative disease-linked mutants strongly suggest that abnormal physical interactions of the mutant proteins with other proteins constitute a cause of disease (22–26). Hence, we next examined the effect of the I93M mutation on the protein interactions of soluble UCH-L1 using a co-immunoprecipitation (coIP) assay. Silver staining of immunoprecipitant revealed that UCH-L1^{WT} interacts with multiple proteins over 30 kDa (Fig. 1E). We found that the amount of each protein interacting with UCH-L1^{I93M} is mostly higher than the amount interacting with UCH-L1^{WT} or other UCH-L1 variants (Fig. 1F; Supplementary Material, Fig. S1B). Monoubiquitin binding of UCH-L1^{I93M} was decreased compared with that of UCH-L1^{WT} (Fig. 1G), consistent with the decreased hydrolase activity of UCH-L1^{I93M} (1,9). However, the cellular monoubiquitin level in cells expressing UCH-L1^{I93M} was not changed compared with that in cells expressing UCH-L1^{WT} (Fig. 1G). Since UCH-L1^{I93M}-associated PD is presumably caused by an acquired toxicity, the toxic function of UCH-L1^{I93M} may not be mainly mediated by a decreased interaction with monoubiquitin, but rather by aberrantly elevated interactions with multiple other proteins.

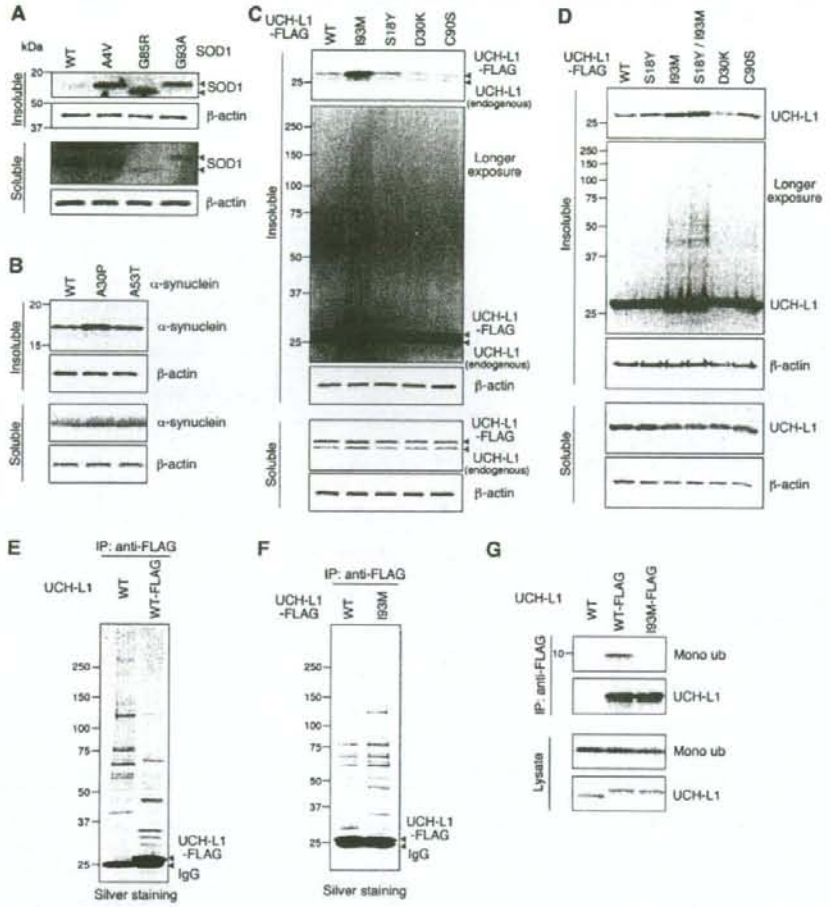

Figure 1. Aberrant biochemical properties of mutant I93M UCH-L1. [(**A**)–(**D**)] SH-SY5Y (A) and (C), Neuro2a (B) and COS-7 cells (D) were transfected with the indicated constructs. Forty-eight hours after transfection, soluble and insoluble fractions were prepared and analyzed by immunoblotting. [(**E**)–(**G**)] COS-7 cells were transfected with the indicated constructs. Cell lysates were immunoprecipitated using anti-FLAG antibody and analyzed by silver staining [(E) and (F)] or by immunoblotting (G). In the presence of FLAG-tagged UCH-L1, UCH-L1-interacting proteins were co-immunoprecipitated with UCH-L1 [(E), lane 2], whereas in the absence of FLAG-tagged UCH-L1, proteins were non-specifically precipitated with anti-FLAG beads [(E), lane 1]. Mono ub, monoubiquitin (G).

Carbonyl-modified UCH-L1 exhibits aberrant properties common to UCH-L1^{I93M}

In the brains of sporadic PD patients, UCH-L1 is a major target of carbonyl formation (12). Carbonyl groups can be introduced into proteins *in vivo* mainly by reactions with 2-alkenals, 4-hydroxy-2-alkenals (HAE) or ketoaldehydes, which are endogenous aldehydic products formed by lipid peroxidation or glycooxidation (27,28). Protein carbonyls can also be produced by metal-catalyzed reactions with H_2O_2 *in vitro* (28,29). To analyze the biochemical properties of carbonyl-modified UCH-L1, we used several carbonyl compounds or H_2O_2 to modify UCH-L1. We have previously reported that UCH-L1 is modified by 4-hydroxy-2-nonenal (HNE) *in vitro* (9). In COS-7 cells transfected with UCH-L1^{WT}, UCH-L1 was modified by physiological concentrations of HNE (10–100 μM) (9) or 4-hydroxy-2-hexenal (HHE) in a dose-dependent manner (Fig. 2A and B; Supplementary Material, Fig. S1C). Carbonyl modification of UCH-L1 was also detected when cells were treated with 100 μM 2-propenal (Fig. 2A), but not with 100 or 500 μM methylglyoxal, 100 or 500 μM malondialdehyde, both of which are ketoaldehydes, or 0.1 or 1 mM H_2O_2 (data not shown). Thus, carbonyl-modified UCH-L1 can be produced by reactions with HAE or 2-alkenals in mammalian cells.

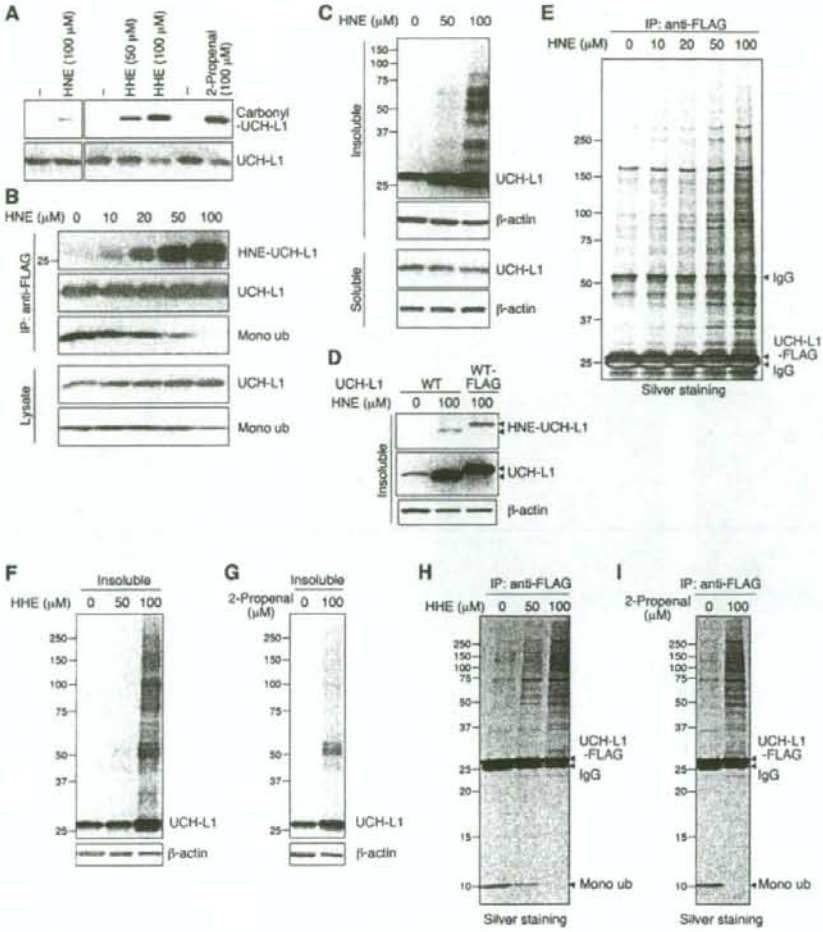

Figure 2. Abnormal biochemical properties of carbonyl-modified UCH-L1. (**A**) COS-7 cells transfected with FLAG-tagged UCH-L1^{WT} were treated with or without the indicated concentrations of carbonyl compounds for 90 min, and immunoprecipitation was performed using anti-FLAG antibody. To detect carbonyl-modified UCH-L1, immunoprecipitants were derivatized with DNPH and immunoblotted using anti-DNP or anti-UCH-L1 antibodies. [(**B**), (**E**), (**H**) and (**I**)] COS-7 cells transfected with FLAG-tagged UCH-L1^{WT} were treated with the indicated concentrations of HNE [(B) and (E)], HHE (H) or 2-propenal (I) for 90 min, and immunoprecipitation was performed using anti-FLAG antibody. Immunoprecipitants were analyzed by immunoblotting or by silver staining. [(**C**), (**F**) and (**G**)] COS-7 cells transfected with FLAG-tagged UCH-L1^{WT} were treated with the indicated concentrations of HNE (C), HHE (F) or 2-propenal (G). Soluble and insoluble fractions were analyzed by immunoblotting. (**D**) COS-7 cells transfected with the indicated constructs were treated with or without HNE, and insoluble fractions were prepared. Immunoblotting shows that the insoluble UCH-L1 that is accumulated upon HNE treatment is modified by HNE.

Interestingly, carbonyl-modified UCH-L1 and UCH-L1^{I93M} exhibit common biochemical properties: ubiquitin binding of HNE-modified UCH-L1 was decreased (Fig. 2B), and both the insolubility of HNE-modified UCH-L1 and the interactions of HNE-modified UCH-L1 with proteins over 30 kDa were increased, compared with those of UCH-L1^{WT} (Fig. 2C–E). HHE and 2-propenal had similar effects to HNE (Fig. 2F–I). Treatment of cells with 100 μM H_2O_2, methylglyoxal or malondialdehyde had no effect on the insolubility of UCH-L1 or the interactions of UCH-L1 with other proteins (data not shown). Consistent with the report that UCH-L1 is a major target of carbonyl formation in the brains of sporadic PD patients (12), UCH-L1 is a major target of carbonyl modification in cells treated with HNE (Fig. 3A). We used the EF1 promoter to yield abundant expression of UCH-L1 in this experiment, since the amount of UCH-L1 is 1–5% of

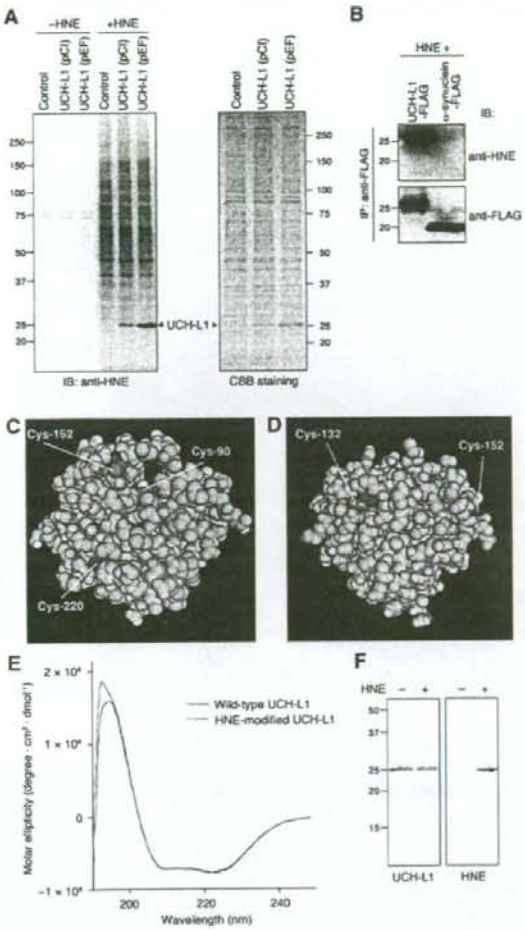

Figure 3. Susceptibility of UCH-L1 to HNE modification and structural properties of UCH-L1 variants. (**A**) COS-7 cells transfected with the indicated constructs were treated with or without 100 μM HNE and analyzed by immunoblotting and CBB staining. (**B**) COS-7 cells transfected with the indicated constructs were treated with 100 μM of HNE, and immunoprecipitation was performed using anti-FLAG antibody. Immunoprecipitants were analyzed by immunoblotting. [(**C**) and (**D**)] Structural model for human UCH-L1. Cys-90, Cys-152 and Cys-220 sidechains are shown in magenta, and backbones are shown in blue (C), using Cn3D software (version 4.1) and NCBI's structural model (mmdbId:38174). Cys-132 and Cys-152 sidechains are shown in magenta, and backbones are shown in blue (D). (**E**) CD spectra (mean residue ellipticity) for recombinant human UCH-L1 proteins. Wild-type UCH-L1 is shown in red and HNE-modified UCH-L1 in blue. (**F**) HNE modification of the recombinant UCH-L1 used in (E) was analyzed by immunoblotting. Modification of UCH-L1 by HNE was detected.

soluble protein in the brain (5). These results suggest that the carbonyl-modified UCH-L1 in sporadic PD brains functions as a causative factor for disease in a similar manner to UCH-L1^{I93M}.

Cys-90 and Cys-152 of UCH-L1 are targets for HAE modification

The appearance of HNE-modified proteins in nigral neurons has been shown to be associated with sporadic PD (30,31). Therefore, we next determined the HNE-modified amino acid residues of UCH-L1 that regulate its insolubility and protein interactions. HNE can form covalent cross-links with cysteine, lysine and histidine residues in proteins (28). To test the specificity of HNE modification in mammalian cells, we used cells transfected with α-synuclein, which contains no cysteine residues. HNE modification of α-synuclein was not detected when cells were treated with 100 μM HNE (Fig. 3B). These results suggest that among the amino acid residues of UCH-L1, cysteine residues are the primary target for HAE. We speculated that Cys-90 is accessible to HAE, since it is accessible to ubiquitin. Using the three-dimensional structure of human UCH-L1 (32), we observed that not only Cys-90 but also Cys-132 and Cys-152 are located on the surface of the protein (Fig. 3C and D). Thus, we tested the insolubility and protein interactions using C90S, C132S and C152S UCH-L1 mutant proteins. We also used C220S UCH-L1 as a control. We found that the C152S mutant bound to monoubiquitin in both HNE-treated cells and untreated cells (Fig. 4A). UCH-L1^{C90S} did not exhibit notably increased insolubility upon HNE-treatment compared with UCH-L1^{WT} (1.3-fold increase in UCH-L1^{C90S}, 2.5-fold increase in UCH-L1^{WT}) (Fig. 4B). The amount of proteins over 30 kDa interacting with UCH-L1^{C90S} was markedly lower than that interacting with UCH-L1^{WT} when cells were treated with HNE (Fig. 4C). Similar results were obtained when cells were treated with HHE (Fig. 4E and F; Supplementary Material, Fig. S1D). Mutations at Cys-132 and Cys-220 had no effect on protein insolubility or interactions (Fig. 4A–C). Consistent with these results, HNE modification of C90S and C152S mutants was decreased compared with that of UCH-L1^{WT} when cells were treated with HNE (~40 and 60% decrease, respectively) (Fig. 4D). These results indicate that HAE modification of UCH-L1 at Cys-90 increases the insolubility and interactions of UCH-L1, and modification of Cys-152 reduces monoubiquitin binding. The level of HNE modification of UCH-L1^{I93M} upon HNE-treatment was markedly lower than that of UCH-L1^{WT} (Fig. 4G). Since the location of Cys-90 is close to Ile-93 (Supplementary Material, Fig. S2), it is possible that the I93M mutation and HAE modification at Cys-90 cause similar structural changes in UCH-L1.

HNE modification causes structural changes in UCH-L1

To address the structural changes in carbonyl-modified UCH-L1, we used CD spectroscopy to estimate the secondary structure. We have previously shown that, compared with UCH-L1^{WT}, the I93M mutant displays lower ellipticity around 195 nm, suggesting a decreased α-helix content, and an increase in the content of β-sheet (9,10). Relative to wild-type protein, HNE-modified UCH-L1 also displayed a lower peak around 190–195 nm (Fig. 3E and F). The relative proportions of α-helix, β-sheet and other secondary structural features in these proteins were estimated from mean residue ellipticity data. HNE-modified UCH-L1 also exhibited

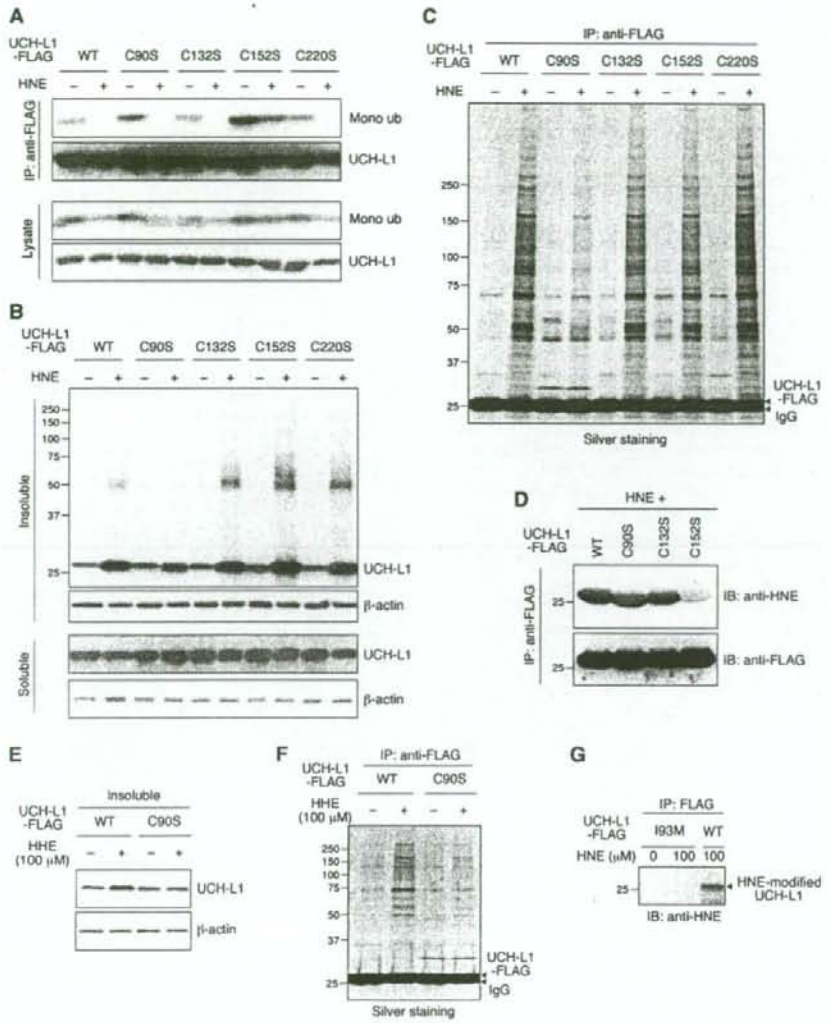

Figure 4. Cysteine residues of UCH-L1 modified by HAE. [(**A**), (**C**), (**D**), (**F**) and (**G**)] COS-7 cells transfected with the indicated constructs were treated with or without 100 μM HNE or HHE. Immunoprecipitation was performed using anti-FLAG antibody, and immunoprecipitants were analyzed by immunoblotting or by silver staining. [(**B**) and (**E**)] COS-7 cells transfected with the indicated constructs were treated with or without 100 μM HNE or HHE. Soluble and insoluble fractions were analyzed by immunoblotting.

decreased α-helix content, and an increase in the content of β-sheet compared with UCH-L1^{WT} (42.9% α-helix, 20.9% β-sheet, 20.6% β-turn and 15.7% random for UCH-L1^{WT}, and 34.0% α-helix, 27.3% β-sheet, 22.3% β-turn and 16.4% random for HNE-modified UCH-L1). These results suggest that UCH-L1^{I93M} and carbonyl-modified UCH-L1 adopt a similar aberrant structure.

The ALS-linked mutation in SOD1 increases its hydrophobicity, which may promote aberrant interactions of SOD1 with other cellular constituents (33). However, the interactions of UCH-L1^{I93M} or HNE-modified UCH-L1 with hydrophobic beads were not altered relative to those of UCH-L1^{WT} (data not shown), indicating that the I93M mutation and HNE modification of UCH-L1 do not increase its hydrophobicity. Considering the fact that unnatural β-sheet proteins readily become insoluble or form further β-hydrogen-bonding with other β-strands they encounter (34), our results suggest that the increased insolubility and protein interactions of abnormal UCH-L1 are due to the increased β-sheet content of UCH-L1.